Long-Term Potentiation and Closed-Loop Learning in Paired Brain Organoids for CNS Drug Discovery

Corey Rountree [1], Eva Schmidt [1], Nicholas Coungeris [2], Victoria Alstat [2], Andrew S. LaCroix [2], Megan Morris [1], Michael J. Moore [1,3], J. Lowry Curley [1]

[1] 28bio Inc, New Orleans, LA

[2] 28bio Inc, Maple Grove, MN

[3] Tulane University, New Orleans, LA

Abstract

Learning and memory, central to cognitive function and critical targets for drug discovery in neurological disorders, fundamentally rely on electrophysiological mechanisms such as short-term potentiation (STP) and long-term potentiation (LTP). We developed an embedded electrode array (EEA) platform supporting electrophysiological integration of paired CNS-3D human brain organoids derived from induced pluripotent stem cells (iPSCs), interconnected via guided axonal growth. Using open-loop stimulation protocols, we demonstrated robust, pharmacologically tunable STP and LTP in trained versus untrained organoid networks, confirmed by pharmaceutical modulation with elevated brain-derived neurotrophic factor (BDNF) enhancing LTP, and NMDA receptor blockade (DL-AP5) preventing its induction. Furthermore, a closed-loop "maze-game" paradigm employing reinforcement learning principles elicited adaptive behavioral responses, demonstrating functional learning capabilities dependent on exogenous BDNF. This integrated platform provides a powerful tool for modeling human synaptic plasticity and cognitive processes *in vitro,* significantly advancing opportunities for therapeutic discovery in cognitive disorders and contributing foundational insights to the emerging field of organoid intelligence.

Introduction

Developing accurate models of human learning and memory is essential for accelerating drug discovery targeting devastating neurological disorders, including Alzheimer's and Parkinson's diseases. Despite intensive efforts, therapeutic development for central nervous system (CNS) diseases face exceptionally high failure rates approaching 100%, largely due to nonpredictive models and biomarkers that fail to accurately predict human efficacy[1,2]. For instance, currently available biomarkers for Alzheimer's disease include amyloid-beta plaques and tau tangles, which typically become detectable years before symptom onset in patients but are most prominent and clearly diagnostic in later disease stages[3]. Although these biomarkers have

significantly advanced our understanding of disease progression, they primarily reflect downstream pathological features rather than directly indicating the underlying functional disruptions that precede cognitive decline[4,5]. Moreover, these pathological features have proven challenging to accurately recapitulate in traditional cellular and animal models, contributing to the high failure rates for CNS-focused drugs[1]. Consequently, there is an urgent need for more functional, human-relevant biomarkers that can robustly predict therapeutic outcomes, accelerating the discovery of effective CNS drugs.

Central to learning and memory are synaptic plasticity mechanisms, particularly short-term potentiation (STP) and long-term potentiation (LTP), which involve activity-dependent strengthening of synaptic connections over the course of minutes-hours or hours-days, respectively[6,7]. Dysfunction in these processes is closely linked to cognitive impairments seen in neurological disorders such as Alzheimer's disease and schizophrenia[8,9]. Although extensively characterized in animal models and isolated human brain slices, investigating LTP and STP directly in human tissues at the scale for drug discovery remains challenging due to limited tissue availability[10,11]. However, recent evidence suggests that these mechanisms could be modeled in human-derived *in vitro* systems[12], indicating the possibility for more accurate functional biomarkers at a scale necessary to screen dozens to thousands of potential compounds.

Three-dimensional (3D) human brain organoids, derived from induced pluripotent stem cells (iPSCs), have emerged as a promising platform to address these challenges[13]. Organoids spontaneously differentiate into complex neural networks containing diverse cell populations, including excitatory and inhibitory neurons as well as critical glia such as astrocytes and oligodendrocytes[14–16]. As they mature, organoids exhibit spontaneous oscillatory electrical activity similar to neonatal EEG patterns, a feature utilized to predict pharmaceutical-induced neurotoxicity[17,18]. Moreover, brain organoids can be genetically or externally induced to model specific neurological conditions, including Alzheimer's disease[19], Parkinson's disease[20], traumatic brain injury[21], autism spectrum disorders[22], and others[23–25]. Recent studies have demonstrated that organoids possess the molecular machinery for synaptic plasticity, as evidenced by their expression of immediate-early genes (e.g., ARC, EGR1) and receptors essential for LTP[12]. While basic forms of synaptic plasticity have been observed[26,27], robust and persistent network-wide LTP remains to be demonstrated. Additionally, the emerging field of organoid intelligence (OI), where organoids serve as biological substrates for computational tasks and cognitive functions, further underscores their potential as sophisticated, clinically-relevant models for studying human neural plasticity and cognitive disorders[28–32]. Establishing platforms to demonstrate pharmacologically modifiable plasticity in organoids would enable more physiologically-relevant *in vitro* metrics and thereby accelerate CNS drug discovery[33,34].

A major challenge in achieving functional potentiation in organoids is the lack of structured connectivity, as higher cognitive functions arise from ensembles of discrete regions interconnected by long axonal tracts. Standard organoid cultures typically consist of isolated organoids cultured without directional cues, limiting the formation of organized synaptic networks. To address this, researchers have begun engineering multi-organoid systems. Assembloids are fused organoids that develop axonal interconnections[35,36]. Others have investigated organoids placed in engineered devices across a separation distance[27,37]. Such organoids interconnected by axons over long distances, or "connectoids," have demonstrated higher order neuronal communication. For instance, Osaki et al. developed a microfluidic platform where reciprocal axon bundles between two cerebral organoids enhanced oscillatory activity and short-term plasticity, demonstrating that structured 3D connectivity boosts functional maturity[27]. These advances allow for more complex neural network dynamics and have led to platforms that can better model synaptic plasticity similar to the different regions in the human brain.

Building on these insights, we developed a novel 24-well embedded electrode array (EEA) platform designed to support paired CNS-3D brain organoids with guided axonal connectivity across extended channels consisting of multiple electrodes. This structured biology enables chronic spatial electrophysiological interrogation of both spontaneous and electrically evoked neural activity. Using learning-inspired stimulation protocols, we successfully demonstrated robust, pharmacologically modifiable STP and LTP within organoid networks. Further, employing a closed-loop "maze game" paradigm based on reinforcement learning principles, we observed adaptive behavioral responses in organoids subjected to signals representing reward and penalty, reflecting functional plasticity and higher-order learning capabilities. Our findings position this organoid-EEA platform as a powerful and versatile *in vitro* model for studying fundamental mechanisms of functional learning and memory, providing a promising tool for drug discovery targeting cognitive disorders and contributing to the emerging field of organoid intelligence.

Results

Paired CNS-3D organoids establish robust axonal growth in EEA plates

Upon placement in the EEA co-culture plate[38], organoid pairs readily extended axons into the connecting channel directed towards one another, achieving physical and functional integration within weeks. Figure 1A shows an immunofluorescence image of a representative day 35 CNS-3D brain organoid[18,39] stained for MAP2 (neurons, green) and GFAP (astrocytes, magenta), illustrating the cell composition and size (~500 µm) of the organoids. The custom 24-well EEA plate (Fig. 1B) allowed two organoids to be positioned in each well with a defined separation. A narrow polyimide microchannel (200 µm width, 500 µm height) guided their neurites to grow

directly toward one another across the intervening gap, wherein ten planar microelectrodes were embedded in the channel floor to record and stimulate the growing axon bundle. We empirically tested three different inter-organoid distances (2 mm, 4 mm, 9 mm) to optimize network formation. Shorter separations promoted faster physical contact between organoids (~1-2 weeks) while longer distances required up to 5 weeks for axon bridging. In practice, all configurations eventually yielded a continuous axon tract linking the organoids, typically within 2–5 weeks of co-culture. The ability to form these "wired" organoid pairs was highly reproducible across ~384 organoid pairs (96 pairs at 2 mm, 120 at 4 mm, 192 at 9 mm). Importantly, the organoid-axon-organoid assemblies remained viable and exhibited oscillatory spontaneous activity and electrically-evoked responses (Fig. 1C), confirming functional integration.

Rapid bidirectional axon extension leads to organoid–organoid connection

Time-lapse brightfield imaging and post hoc immunostaining revealed the spatiotemporal progression of axon growth through the EEA channel (Fig. 2). Figure 2A presents a montage of brightfield images from a representative organoid pair with 9 mm separation over its first five weeks in co-culture (day *in vitro*, DIV 3 to DIV 35). In the initial days, individual neurites emerged from each organoid into the proximal end of the channel. By one week (DIV 7), there was a dense web of fibers near each organoid, evident as bundle-like structures extending into the channel (Fig. 2A, DIV 7, red inset). From week 2 onward, these axonal fronts continued to elongate and eventually converged at the mid-channel (orange inset), establishing physical contact between organoids with increasing fiber density through DIV 35. By DIV 35, the phase-contrast image shows an obvious tissue strand spanning the entire channel. Correspondingly, immunofluorescence labeling for β-III tubulin at 9 weeks to highlight axonal fibers (Fig. 2B) confirmed a continuous, fasciculated axon bundle bridging Organoid 1 and Organoid 2 (insets highlight the tightly bundled tract at each organoid and in the mid-channel). We noted that axons intermingled within this bundle, creating a potential feed-forward and feedback loop between the two organoids.

To quantify outgrowth kinetics, we measured fiber density over time in three regions: near Organoid 1 (red zone), the channel midpoint (yellow), and near Organoid 2 (blue). Figure 2C plots the normalized fiber density versus time for young organoids (1 week old at placement in the EEA plates) and more mature organoids (5 weeks old at placement in the EEA plates). In all cases, axonal extension followed a sigmoidal growth curve with an initially rapid phase that plateaued as the channel filled. As expected, fibers reached 50% of maximal density significantly sooner in regions closer to the organoids than in the mid-channel. The half-maximal outgrowth times (EC_{50}) in the organoid-adjacent regions were about 2–3 times faster than at the channel center, reflecting that axons sprout quickly from the organoid surface and then gradually

populate the distal gap. By the end of week 5, organoid-adjacent regions achieved a higher overall fiber density compared to the mid-channel, especially for the older organoid cohort. Nevertheless, both young and mature organoids ultimately formed robust inter-organoid tracts. Together, these data demonstrate that two independently grown organoids can be linked via a self-assembled axonal bundle. The maturation rate of this "mini-circuit" depends on both the developmental stage of the organoids and the distance between them, but even relatively immature organoids are capable of projecting long axons and establishing a connected bridge within a few weeks that becomes denser over time.

Emergence of network activity and stimulus responsiveness

Having established structural connectivity, we examined how functional activity in the organoid networks evolved longitudinally with extended culture timelines. Using the embedded electrodes, we recorded spontaneous electrophysiological activity from organoid pairs over multiple weeks with a custom electrophysiology system (Figure 3A). Figure 3B tracks the development of network bursts in a representative organoid pair from 1 to 3 weeks *in vitro* (DIV 6–20). Kernel density estimates of burst frequency are plotted for an electrode beneath one organoid (green) versus an electrode at the channel midpoint (blue). Early on (around 1 week), the organoid shows intermittent, small bursts, while the mid-channel region is mostly silent (no established connection yet). By DIV 13 (~2 weeks), a clear change occurs: high-amplitude bursting is observed under the organoid with increased regularity, and bursts now also appear on the mid-channel electrode. This coincides with the initial detection of axonal connection between organoids. By DIV 20 (~3 weeks), both the organoid and midpoint electrodes exhibit robust network activity arising from one or both organoids. These results align with previous reports that inter-organoid connections can amplify network dynamics. In our experiments, organoid pairs consistently showed a marked increase in burst intensity and frequency once the axon bundle formed.

We quantified burst rates across multiple organoid pairs and related it to organoid age and initial maturity. Figure 3C summarizes the mean number of bursts per 10 min recording as a function of time in culture, comparing organoids that were seeded into the EEA plates at 1-week-old vs. 5-weeks-old. Both cohorts exhibited an upward trend in burst frequency over weeks of co-culture, reflecting ongoing network maturation. The overall activity was higher in the cohort that started with 5-week-old organoids, as expected given their more advanced neuronal development. These trends are in line with prior calcium imaging studies showing similar bursting rates of CNS-3D organoids at similar time scales. Thus, within our platform, organoid pairs achieve self-organized oscillatory activity that intensifies with age, and the presence of inter-organoid connections does not impede the intrinsic maturation of bursting.

We next sought to reliably evoke electrophysiological responses from the organoid networks to probe their functional connectivity and excitability. Using the stimulation paradigm detailed in the Methods, we conducted a systematic probing of stimulation parameters to identify those that best elicited reproducible neural responses (Fig. 3D). The parameter space included current amplitude, pulse width, polarity, pulse number, and frequency. Each condition was evaluated for its capacity to elicit time-locked action potential responses. Figure 3E shows example evoked responses under different conditions. In some cases, a given stimulus produced no response (Fig. 3E, left), indicating either that the stimulated site was not closely integrated with the neuronal network or that the parameter set was not appropriate. In other cases, a single pulse could trigger a robust burst of spikes (Fig. 3E, middle), often involving multiple units firing within a few milliseconds post-stimulus - a sign of functional recruitment of a local microcircuit. We also observed graded responses when varying stimulus intensity: the rightmost panel of Fig. 3E overlays responses to a series of pulses with increasing current (200 to 400 uA), showing incremental spike recruitment with more spikes as current rises. These profiles are reminiscent of input-output curves in traditional brain slice experiments, where stronger stimulation aggregates more responsive neurons[40]. After systematically exploring stimulus parameters (Fig. 3D), we identified the conditions yielding the most consistent, time-locked activation of the organoid pairs. Figure 3F summarizes the outcome of this screening: among dozens of tested parameter combinations (pulse widths, amplitudes, etc.), two conditions stood out (red arrows) that evoked reproducible spiking on >80% of trials and these conditions were selected for subsequent experiments: a short duration, high current pulse (100 us, 400 uA) and a long duration, low current pulse (500 us, 100 uA).

Using this stimulus, we compared the evoked responsiveness of younger vs. older organoid networks. We found that organoid age did not strongly influence evoked spike yield under our conditions. As shown in Figure 3H, the average number of spikes evoked per stimulus was comparable between networks that had been placed at 1-week-old and those placed at 5-weeks-old both tested after 5 weeks of growth in the EEA plates. Statistical analysis confirmed no significant difference between the two groups' evoked response magnitudes. This suggests that by the time of these assays (typically 6–10 weeks of total organoid age), both younger-start and older-start networks achieve a similar level of functional connectivity and excitability in response to external input. We therefore pooled data across ages for subsequent plasticity experiments.

We finally performed spike sorting on recorded multi-unit data to assess the complexity and stability of neural signals across the organoid–channel network. As shown in Figure 3H, wavelet clustering of waveforms from a single electrode revealed multiple distinct clusters, each corresponding to a presumptive single unit[41]. This pattern was observed across several electrodes in the system, indicating that we were recording from multiple individual neurons at

once. The ability to resolve and track multiple units supports the conclusion that our platform samples activity from a distributed population of neurons, consistent with the formation of a functional neuronal network across the paired organoids. Together, results from Fig. 3 establish that our organoid pairs can generate reliable metrics of network activity, both spontaneous (bursting) and evoked (stimulus responses). These metrics establish a baseline against which we can detect any training-induced potentiation or changes in synaptic function.

Induction of short-term potentiation (STP) via repeated open-loop stimulation

We first examined whether short-term stimulus training could enhance the neural activity of organoid networks as an *in vitro* analog of STP. For this, we implemented an open-loop training paradigm over the course of one week, as described in Methods and Fig. 4A. Each day, trained organoids received a series of stimuli (five rounds of pulsing all electrodes), whereas untrained controls did not, while both were evaluated before and after training to measure any changes in evoked spiking. Figure 4B provides a qualitative example of the outcome from untrained (top) and trained (bottom) wells. Spike plots show that initially (Evaluation #1) the organoids exhibited relatively sparse firing in response to test stimuli and after the training session (Evaluation #2) the trained well, but not the untrained well, displayed markedly more action potentials post-stimulation. This indicates a potentiation of responsiveness induced by the training of that day over the course of ~30 minutes between evaluations.

To aggregate results across experiments, we calculated a potentiation ratio for each day defined as the total spikes in Evaluation #2 divided by total spikes in Evaluation #1 for that day for each well. Figure 4C plots these normalized spike counts for all plates (N = 19) over the training week. A clear distinction is evident: the trained cohort consistently showed a >100% ratio (meaning spiking increased from pre- to post-training), whereas the untrained cohort hovered near 100% (no change) or below (slight rundown). By the end of the week, trained organoids had on average ~1.5–2 times the evoked spike output after training relative to before, a significant elevation over untrained controls ($p < 0.05$, t-test). We refer to this increase as short-term potentiation (STP) because it developed rapidly within minutes of stimulation. Importantly, the potentiation appeared to be timing independent: the trained networks displayed the same STP effects both during training over consecutive days and over the weekend gap.

To probe the dependence of this short-term potentiation on specific pathways, we tested the effects of two pharmacological agents during the training week: elevated (50 ng/mL compared to the usual 20 ng/ mL) BDNF (brain-derived neurotrophic factor; a facilitator of synaptic potentiation) and DL-AP5 (an NMDA receptor antagonist that blocks canonical LTP induction). Neither agent drastically altered the STP observed over 1 week. As shown in Figure 4D, in standard control medium the trained group had significantly higher normalized spike counts than untrained at the end of the week (average over training days 2–4) consistent with Fig. 4C.

This training effect was equally present when 50 ng/mL BDNF was added to the medium and also when 200 µM DL-AP5 was included (with trained > untrained in both cases, $p < 0.05$). In other words, regardless of treatment, the act of training conferred a boost in evoked spiking relative to no training. Moreover, when comparing across treatments, we found no significant difference in the degree of potentiation: spike count increases from training in the BDNF-supplemented group were comparable with those in control medium, and DL-AP5-treated organoids showed a similar potentiation magnitude as well. Statistical analysis confirmed that within each treatment condition, the normalized potentiation of trained vs. untrained did not significantly deviate from the control condition. These results indicate that the short-term network potentiation was largely insensitive to acute modulation of TrkB or NMDA receptor signaling[42].

Induction of long-term potentiation (LTP) and pharmacological modulation

To evaluate whether stimulation induced long-lasting changes in network excitability consistent with LTP, we quantified changes in the evoked spike counts from day-to-day using data from Evaluation #1 alone. Figure 5A shows spike plots from two representative wells from untrained (top) and trained (bottom) groups, illustrating increased evoked responses across successive days in the trained organoid pair but not the untrained pair. At the population level, we quantified LTP as the ratio of evoked spikes on each day relative to the Day 0 baseline for trained versus untrained groups. Figure 5B shows the mean normalized spike count trajectories over the training week for three conditions: control medium, BDNF-supplemented, and DL-AP5-treated. In control conditions, the trained organoids exhibited a significant increase in evoked spikes compared to untrained by Day 2, and this potentiation became larger by Day 3–4 (trained reaching ~1.9-fold baseline vs. untrained ~0.8-fold). The separation between trained and untrained was significant on Days 2–4 ($p < 0.05$) and persisted through the end of the week. Notably, when elevated BDNF was added (50 ng/mL), the rate and extent of potentiation were even greater: trained organoids in BDNF climbed to ~3-4× baseline by Day 4, nearly double the level of the trained control group. This suggests that exogenous BDNF provided an additional boost, possibly by lowering the threshold or enhancing the magnitude of synaptic strengthening events. In contrast, NMDA receptor blockade with DL-AP5 completely prevented any training effect - the trained and untrained curves under DL-AP5 were indistinguishable throughout the week (both around ~1.1–1.5× baseline, with no significant difference), consistent with NMDA receptor activity being required for the induction of sustained LTP. These divergent outcomes highlight that the potentiation we observed after extensive training corresponds to long-term potentiation, as opposed to nonspecific increases, given its dependency on NMDA receptor-mediated mechanisms.

To assess the stability of this potentiation, we continued evaluation after a two-day pause with no stimulation. In the control condition, trained cultures showed a partial reduction in spike output by Day 7, indicating that potentiation was not fully maintained without ongoing stimulation. This decay pattern is characteristic of early-phase LTP (E-LTP), which is known to last hours to days and typically decays in the absence of protein synthesis or further reinforcement. By contrast, in the BDNF-supplemented condition, trained cultures showed a decrease in activity but still maintained significantly elevated spike counts after the weekend pause, suggesting that BDNF promotes the stabilization and persistence of potentiation. This prolonged effect is consistent with a transition toward late-phase LTP (L-LTP), which involves long-term structural or molecular changes and is dependent on neurotrophic signaling pathways.

We compared end-of-week metrics across conditions (Fig. 5C) by averaging the normalized spike counts from days 2-4 (Wednesday-Friday) of the week. We found that the average normalized spike count for trained organoids in control and BDNF+ conditions was significantly higher than that in DL-AP5-treated organoids. Similarly, we examined the number of active neurons detected via spike sorting in each condition (Fig. 5D) comparing trained vs untrained samples for each dosing condition. In both control and BDNF groups, the trained organoids exhibited a larger count of distinct neurons contributing spikes by the end of training compared to untrained, whereas under DL-AP5 the trained and untrained had equally low counts.

Closed-loop "Maze-Game" paradigm for organoid learning

Having shown that patterned stimulation alone could induce plasticity, we next evaluated whether organoid pairs could learn to modify their activity in response to reward or penalty feedback. We designed a neural interface for the organoids with a custom-designed "maze game" under a closed-loop protocol broken into learning and memory phases (Fig. 6A), effectively treating the organoid pair as a living agent navigating a simple environment. In this setup, the organoid could only influence the game through its neural responses to stimuli, which the controller translated into directional movements, and in turn the organoid received sensory consequences in the form of stimuli representing "reward" or "penalty". This embodied closed-loop format is conceptually similar to recent studies where neural cultures learned to play games when given feedback[28,31].

Figure 6B outlines the maze layouts used. During evaluation trials (before and after training), a fixed evaluation maze was used for all organoids, containing "food" and a single pursuer (virtual cat) at specific locations. During training trials, four smaller mazes were used (Fig. 6B, bottom), each being a rotated version of simple binary decisions (two directions leading to food, the other two to danger). This prevented any directional bias as each cardinal direction had an equal chance to be correct across trials. The training mazes also forced the organoids to experience both rewarding and penalizing outcomes. The legend in Fig. 6B defines the tile types

and their associated stimuli. We crafted a library of stimuli (Fig. 6C) such that each tile or event corresponded to a unique electrical input pattern. For instance, when the cursor was adjacent to the food tile, a specific "food proximity" stimulus was delivered on electrodes corresponding to the direction of the food. Contact with the food tile triggered a reward stimulus, represented by a rest period without stimulation intended to reinforce whatever neural activity led to that success. Conversely, approaching the danger tiles elicited a "danger proximity" stimulus, and moving onto it triggered one of two penalty stimuli (see below for details) as a form of negative reinforcement. Importantly, the intensity (i.e. current amplitude) of these stimuli was attenuated with distance: for every grid step farther from a tile, the stimulus current was reduced by 25 µA per step. Thus, the system was designed so that the organoid network would receive a gradient of stimulus strength indicating how close it was to a goal or hazard, an element akin to sensing in a real environment. All stimuli were delivered as biphasic pulses or pulse trains on designated electrode pairs, targeting both organoids and/or the channel as appropriate to engage a broad network response (Fig. 6C table lists the stimulus types and parameters).

The closed-loop control cycle (Fig. 6D) ran continuously during a maze or training trial. In each step, the system applied four directional stimuli simultaneously (up, down, left, right) and listened to the organoid activity for ~0.1 s. Because these stimuli were spatially separated on different electrode pairs, the organoid's response could exhibit bias toward one direction (e.g. higher firing on electrodes associated with "up"). The controller then moved the cursor in the direction that elicited the highest neural firing rate. This effectively means the organoid "chooses" the direction by generating more activity in response to that directional cue. We note that initially, these choices may be random or reflect innate biases in connectivity (e.g., one organoid might be more responsive to stimuli on a certain side or show a preference to move towards danger), but with training, the goal was to see if the organoid could learn to favor the direction leading to reward (food) over that leading to penalty (danger). After the move, if a reward or penalty condition was met, the corresponding stimulus was delivered, which could further alter the network state, and if the trial ended (by reaching food or danger or timeout), the next trial would start after a short inter-trial interval. Each organoid pair's performance was tracked over multiple trials to assess learning in the form of the points scored for contacting food or survival time in game iterations, both measured as best across three repetitions.

Using this closed-loop framework, we compared a trained group, which underwent the full maze training regimen, to an untrained group that only did the evaluation runs without any intervening training. Additionally, within the trained group, we tested two different penalty feedback strategies: Penalty #1 was a single, inverted polarity danger stimulus and Penalty #2 was a more intense burst of 5 high-frequency danger-like pulses (Fig. 6C). The rationale was to see if a stronger punishment signal (Penalty #2, involving high-frequency stimulation known to

drive plasticity) would be more effective for learning than a weaker one (Penalty #1) that seemed aversive due to lack of responses (Fig. 3F). Both paradigms used the same reward stimulus for consistency.

Goal-directed learning behavior and BDNF-dependent memory in organoids

Across two weeks of closed-loop training, we found that organoid pairs receiving the Penalty #2 paradigm (high-frequency burst punishment) showed significant signs of performance improvement, whereas those receiving the Penalty #1 paradigm did not. Figure 7A plots the raw and normalized point totals for three groups – untrained, trained with Penalty #1, and trained with Penalty #2 – over the average learning and memory weeks. Upon initial observation, the raw performance (Fig. 7A left; best points scored across 3 maze runs) of the groups show substantial overlap but the scores for Penalty #2 became significantly elevated compared to untrained by the end of the week. When normalized to each group's Day 0 baseline (Fig. 7A, middle), a trend appeared as early as Day 2 where the Penalty #2 group demonstrated a significant, monotonic increase over time, whereas the other groups showed little or no upward trend. This was corroborated by examining the average performance metrics (Fig. 7A right) at the end-of-week by averaging the normalized values for each condition across days 2-4. The end-of-week analysis confirmed that only Penalty #2 induced significant improvement in learning, a benefit that was lost in the memory phase without continued reinforcement. Survival time outcomes mirrored these findings (Figure 7B), with Penalty #2 extending survival progressively during learning, while Penalty #1 provided a smaller, but significant, benefit. No group differences were observed in memory, highlighting the transient nature of the learning effect.

Next, we compared organoid learning under normal control media versus BDNF-depleted conditions to determine the possibility for pharmacological modulation. As shown in Figure 7C, organoids trained with Penalty #2 in our standard medium (supplemented with 20 ng/mL BDNF) displayed a significant improvement in both total points (left) and survival time (middle) relative to untrained controls. However, when the same training protocol was applied to organoids in BDNF-free medium, the trained networks no longer outperformed the untrained with points and survival time equivalent to untrained controls. This is shown directly in the right panel of Figure 7C, where the control medium condition is compared to a BDNF- condition by averaging data across days 2-4 (end-of-week).

Discussion

In this study, we introduced a versatile brain organoid model integrated with electrophysiology and demonstrated that it can capture core hallmarks of learning and memory, specifically long-term synaptic potentiation (LTP) and goal-directed adaptive behavior, in CNS-3D organoids. Our

approach leveraged the integration of two brain organoids via a guided axonal tract on an embedded electrode array (EEA), allowing us to electrically stimulate and record distributed neural activity over weeks of development. The results establish several key findings: (1) Paired organoids form functional axonal connections, consistent with recent "connectoid" models[27,37]. (2) Repeated patterned stimulation induces a training-dependent increase in neural activity that can persist for minutes (STP) and become sustained over longer periods as LTP, mirroring the fundamental plasticity behavior of neurons *in vivo*[43]. (3) This LTP is pharmacologically tunable – it is accelerated by elevated BDNF and abolished by NMDA receptor inhibition, indicating that the organoid network engages canonical molecular pathways for plasticity[7,44]. (4) When embodied in a closed-loop feedback loop, organoid networks are capable of learning a rudimentary task by navigating toward a reward in a virtual maze, especially when provided with appropriately strong feedback stimuli. However, this learned behavior is transient and dependent on neurotrophic support via exogenous BDNF, suggesting that the memory trace in organoids is fragile and perhaps analogous to short-term memory that requires continual reinforcement[45]. We discuss the implications of these on neuroscience and drug discovery below.

A central achievement of this work is the induction of LTP in a multi-organoid system connected via axonal tracts, tested with pharmacological modulation. Our experiments revealed a clear distinction between short-term potentiation (STP) and LTP in organoid networks matching up with literature[12,27,46]. STP, defined here as increased evoked activity within the same day following repeated stimulation, was observed across multiple wells and was reproducible. Importantly, STP was not significantly affected by BDNF supplementation or NMDA receptor blockade with DL-AP5, suggesting that it arises from presynaptic mechanisms such as residual calcium accumulation, increased neurotransmitter availability, or short-term synaptic facilitation[47]. These mechanisms are well-documented in other systems and typically support potentiation over the course of minutes to a few hours, independent of protein synthesis or neurotrophic modulation[47,48]. In contrast, LTP, defined by potentiation that persisted across days, was abolished by DL-AP5 and enhanced by elevated BDNF, consistent with classical NMDA receptor-dependent and neurotrophin-facilitated mechanisms. This two-stage model (NMDA-independent early potentiation, NMDA-dependent late phase) aligns with classic early-LTP vs. late-LTP descriptions and underscores the complexity of plasticity even *in vitro*[12,45]. Together, these findings highlight that our organoid-electrode system captures multiple temporal phases of synaptic modulation: a fast, NMDA-independent potentiation likely driven by presynaptic factors, and a slower, durable form consistent with early- to late-phase LTP that is sensitive to pharmacological modulation.

The ability to study a human 3D model of LTP opens new avenues for translational biomedical research and as a step toward biocomputing with living networks. Drug discovery for cognitive

enhancement or neuropsychiatric conditions often suffers from the gap between animal models (e.g. rodent, non-human primate, etc) and human outcomes. A human organoid model that exhibits LTP could be used to screen compounds that promote or inhibit synaptic plasticity. For instance, nootropics or novel NMDA receptor modulators could be applied to organoids to see if they prolong LTP, mimicking potential pro-cognitive effects[49]. Likewise, models of disease (e.g., organoids derived from patients with Alzheimer's or autism) could be tested for deficits in LTP induction and potential rescue by therapeutics, providing a phenotypic assay for synaptic dysfunction in a patient-specific context[50]. These are applications that current animal models only approximate, but an organoid model might address with human biology. Moreover, the multi-well format of our platform represents a first step in scalability establishing the feasibility of parallel experiments with the existing 24-well plate that could be expanded to increase the number of wells or organoids per well to accomplish higher-throughput or more complex biological models, respectively.

Future research could further enhance this approach in several important ways. First, the variability inherent in organoid cultures is nontrivial. While the CNS-3D organoids are initially very uniform in size and cellular composition, differences in proximity to the electrodes or differing axonal growth rates in the EEA plates can lead to variability in outcomes (e.g., some organoid pairs responded more strongly to training than others). We partially addressed this by using cohort averaging and normalization but improving consistency will be important for translational use. Second, our current demonstration of learning is limited to a relatively short-term improvement that fades without reinforcement. Achieving long-lasting memory storage *in vitro* may require additional strategies, such as longer training periods, incorporation of myelinating cells (to facilitate faster communication and perhaps more stable circuits), or stimulation paradigms that mimic sleep consolidation[51]. Third, the scale of our organoid networks is modest compared even to a rodent brain (~68 million neurons in mice; ~188 million neurons in rats), on the order of 25k neurons per organoid[52]. This is sufficient for the simple tasks here, but more complex behaviors or computational tasks might require more complex or multiple interconnected organoids. Finally, we note an ethical consideration: as organoids gain complexity and exhibit more brain-like activity such as learning, questions arise about their potential for sentience or pain perception. Our maze-game is a rudimentary setup with abstract "rewards" and "penalties," and there is no evidence that these stimuli cause anything like pain; however, we remain cognizant of ongoing ethical dialogues around organoid intelligence. We support an embedded ethics approach, engaging ethicists and the public as we push the boundaries of what organoids can do[53,54].

In conclusion, our findings underscore the remarkable potential of combining 3D human brain organoids with engineered neural interfaces to create functional *in vitro* models of learning and memory. We successfully induced long-term potentiation in an organoid network, a milestone

indicating that these brain organoids share functional plasticity mechanisms with real brains. Furthermore, by closing the loop between an organoid and a computer-simulated environment, we demonstrated a nascent form of goal-directed learning in a biological system derived from human cells. This convergence of tissue engineering, electrophysiology, and computational feedback heralds a new avenue for neuroscience research: one where we can experimentally teach an *in vitro* human neural network and watch it learn. In the near term, this platform can be applied to screen drugs that enhance or impair memory at the cellular level, providing insight into treatments for cognitive disorders such as Alzheimer's disease. In the longer term, improvements in scale, complexity, and interfacing may allow organoid-based systems to tackle computational problems or serve as biological data storage complementing artificial intelligence and digital data centers, respectively. As we refine these technologies, we move closer to realizing organoid intelligence: an interdisciplinary frontier where lab-grown human brain organoids compute, remember, and perhaps one day exhibit forms of intelligence that can enable life-changing biomedical research and technological breakthroughs.

Figures

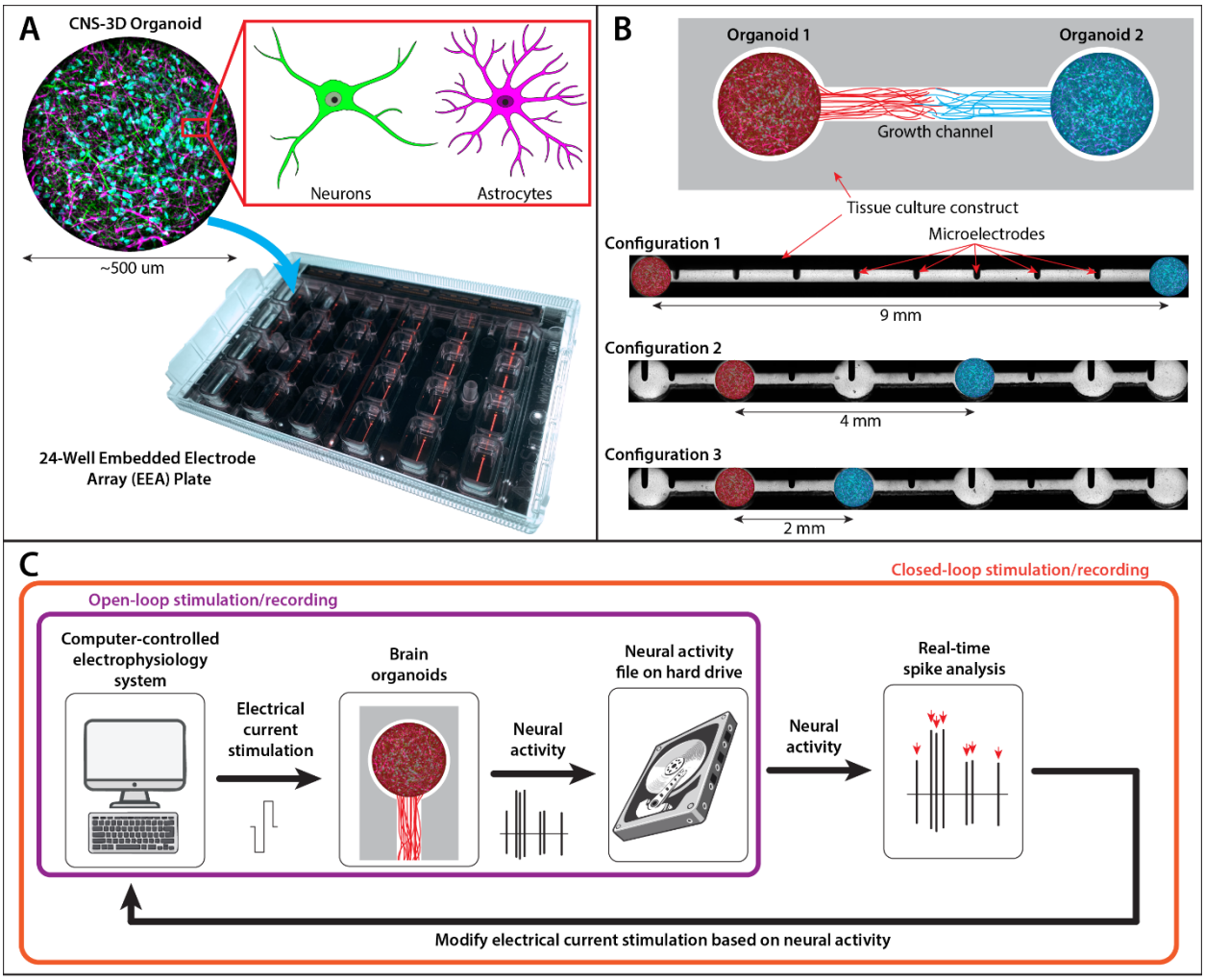

Figure 1. Platform for electrically interfacing paired CNS-3D brain organoids
A) Immunofluorescence micrograph of a human iPSC-derived CNS-3D brain organoid (~500 µm Ø) composed predominantly of cortical neurons and astrocytes (representative markers: MAP2 [green] & GFAP [magenta]). **B)** Schematic of the custom 24-well embedded-electrode array (EEA) plate used for dual-organoid co-culture. Two organoids are positioned in each well and linked by a growth channel that guides axonal projections across ten planar microelectrodes embedded in the channel floor. Three inter-organoid separations were tested: Configuration 1 = 9 mm, Configuration 2 = 4 mm, and Configuration 3 = 2 mm. **C)** Block diagram of open-loop (purple) versus closed-loop (orange) stimulation paradigms. Open-loop delivers predefined current pulses to electrodes and records the evoked neural activity for offline analysis. Closed-loop performs real-time spike detection on recorded signals and dynamically adjusts subsequent stimulation parameters based on the detected activity.

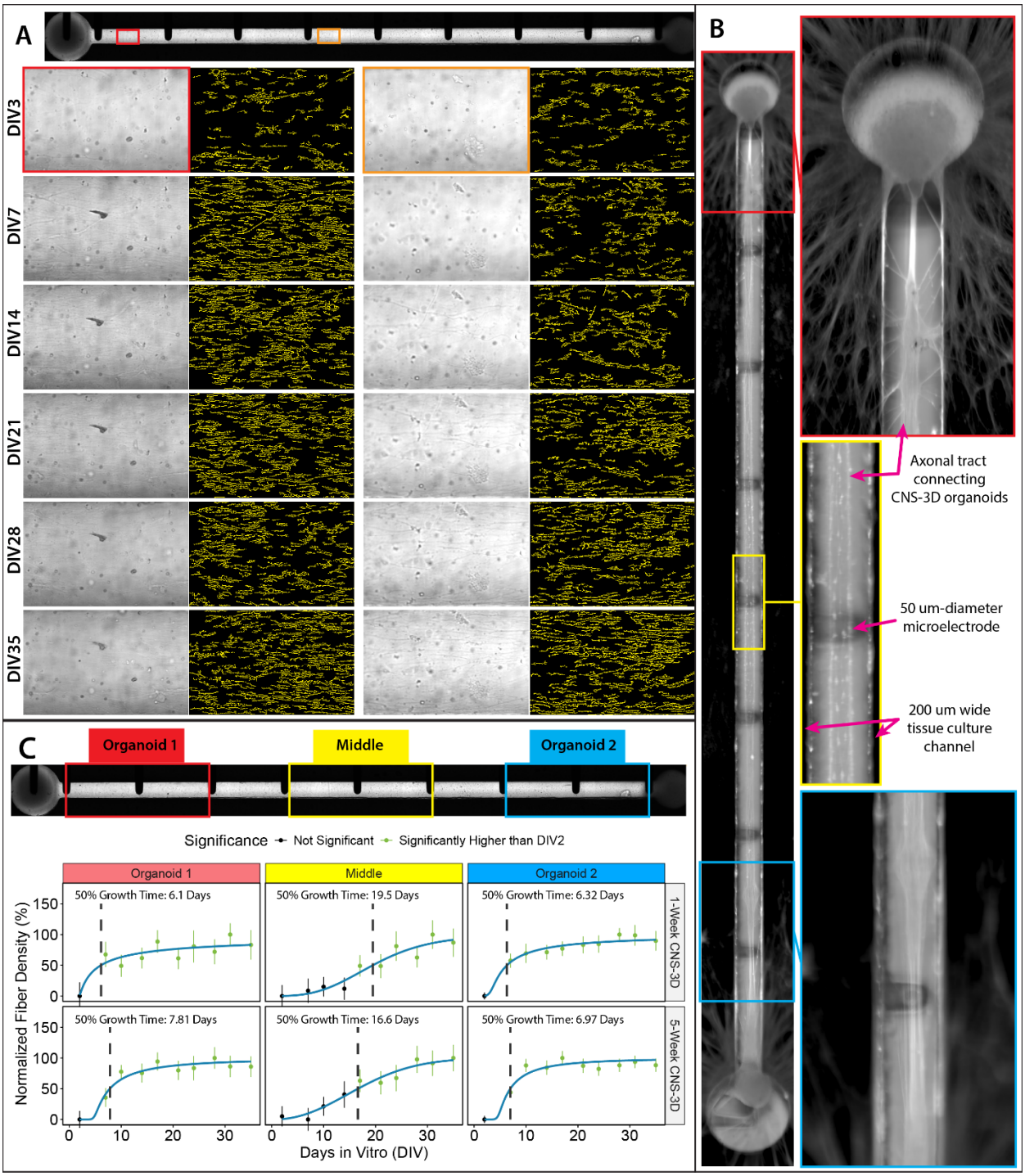

Figure 2. Spatiotemporal dynamics of axonal outgrowth in the embedded-electrode array (EEA) channel

A) Brightfield montage of a representative 1-week-old CNS-3D organoid pair (day in vitro, DIV 3–35). The red and orange boxes mark regions adjacent to Organoid 1 and the channel midpoint, respectively. For each region, brightfield closeups (left) and niBlack-filtered fiber masks (right)

illustrate rapid fiber densification near the organoid by DIV 7, followed by progressive infill of the mid-channel through DIV 35. **B)** Whole-channel immunofluorescence (β-III-tubulin) highlighting Organoid 1 (red), channel midpoint (yellow) and Organoid 2 (blue). Insets reveal a continuous, fasciculated axon bundle bridging the two organoids. **C)** Quantitative fiber-density trajectories (mean ± SEM, normalized to maximum) for the three regions. Top: 1-week organoids; bottom: 5-week organoids. Sigmoid fits (blue lines) yield EC_{50} values (time to 50 % max density; black dashes) showing regions near the organoids reach max density about 2-3 times faster than the middle of the channel. These data show that axons extend rapidly from each organoid and converge to form a robust, bidirectional nerve bundle whose maturation rate depends on both organoid age and channel position.

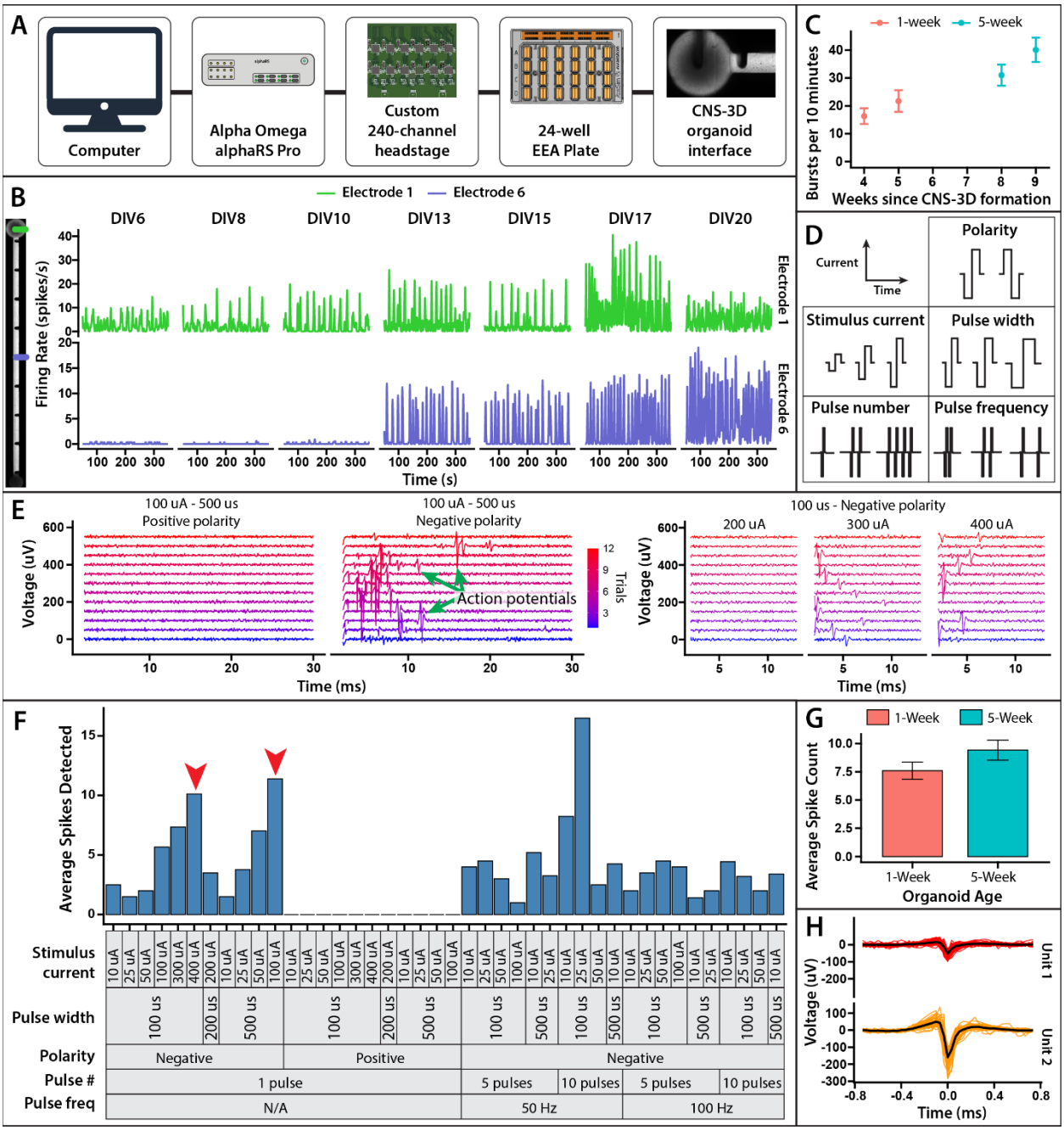

Figure 3. Characterization of spontaneous and electrically evoked activity in paired CNS-3D organoids

A) Hardware chain for closed-loop electrophysiology. A control PC drives an Alpha-Omega αRS-Pro stimulator/recorder, a custom 240-channel headstage, and a 24-well embedded electrode array (EEA) plate; each well contains two CNS-3D organoids positioned over ten planar electrodes. **B)** Development of spontaneous network bursts. Kernel-density estimates of burst rate recorded from an electrode beneath an organoid (green) and a midway channel electrode

(blue) in a representative 5-week culture. Bursting beneath the organoid increases in amplitude and regularity from DIV 6-20, whereas mid-channel bursts appear at DIV 13, reflecting progressive axonal innervation. **C)** Cohort-level maturation. Mean ± SEM number of bursts detected during 10-min recordings versus organoid age (weeks since formation) for cohorts seeded at 1-week (red) and 5-weeks (blue). Trends parallel previously reported FLIPR Ca^{2+} activity of CNS-3D organoids at matched ages. **D)** Parameter space explored for electrical stimulation included: stimulus current, pulse width, initial polarity, pulse number, and pulse frequency. **E)** Representative evoked responses. Overlays of 12 identical trials illustrate a non-response (upper left), a robust multi-unit response (upper right), and a current-ramp series (bottom) showing graded recruitment with increasing current. Trials are vertically offset for clarity with different colors representing early (blue) vs late (red) trials. **F)** Screening outcome. Bar graph summarizes evoked spike counts for every parameter combination (table beneath). Two conditions, 100 µs + ≥300 µA and 500 µs + 100 µA, produced the most consistent, time-locked responses (highlighted) and were selected for all subsequent experiments. **G)** Evoked responsiveness across development. Average spikes ± SEM elicited by the 500 µs, 100 µA paradigm show comparable magnitudes in the 1-week and 5-week cultures (n.s., two-tailed t-test). Therefore, data were pooled for later analyses. **H)** Example spike sorting results following wavelet clustering yields two single-unit waveforms (Unit 1, Unit 2) that were tracked across all subsequent analyses. Together, these results establish reliable metrics for tracking spontaneous network maturation and identify stimulation parameters that evoke robust, stereotyped activity in CNS-3D organoid pairs.

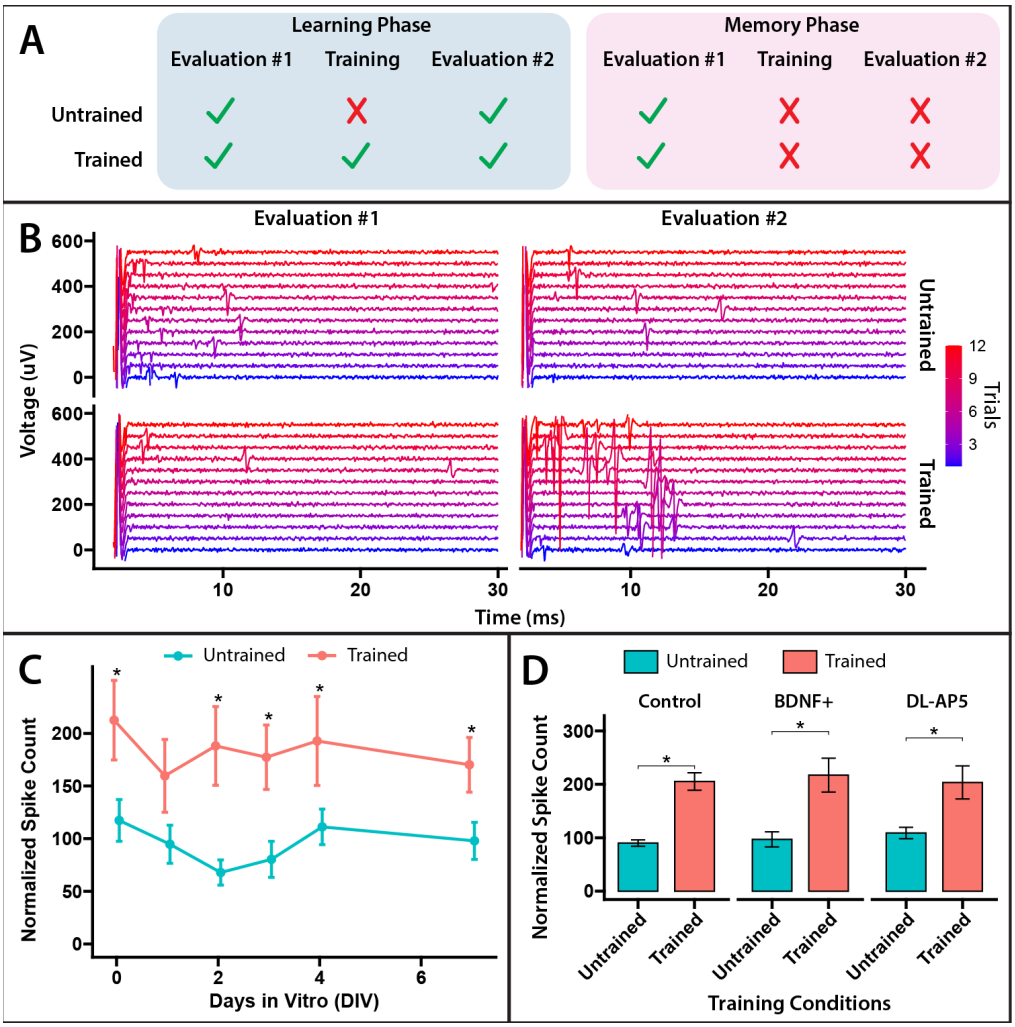

Figure 4. Short-term potentiation (STP) induced by open-loop training

A) Experimental timeline for the STP and LTP experiments. Learning phase: both untrained and trained cohorts complete Evaluation #1 (stimulation at each organoid separately and together). The trained cohort then undergoes repeated training consisting of 5 rounds of stimulation at all electrodes before both cohorts perform Evaluation #2 (repeat of Evaluation #1). The learning phase is repeated each weekday for one week. Memory phase: The subsequent week, both cohorts are tested identically in a single evaluation for each weekday over one week. **B)** Representative spike plots from untrained (top) and trained (bottom) wells showing evoked activity during Evaluation #1 (left) compared to Evaluation #2 (right). The untrained sample shows no increase in activity while the trained sample shows an increase in observed action potentials after training in Evaluation #2 compared to Evaluation #1. **C)** Population level STP comparison. Normalized spike count (spikes @ Eval 2 / spikes @ Eval 1; mean ± SEM) for all plates, wells, and days shows a significant elevation in the trained cohort versus untrained ($p < 0.05$, t-test). The potentiation persists across the weekend pause (gap between Days 4 and 7).

D) Pharmacological modulation of STP. At the end of the learning week (Days 2 - 4), trained organoids display significantly ($p < 0.05$, t-test) higher normalized spike counts (mean ± SEM) than untrained in control medium, in the presence of elevated BDNF (50 ng mL^{-1}), and under NMDA-receptor blockade with DL-AP5 (50 µM). These data demonstrate a robust, training-dependent short-term potentiation of spiking activity that was repeatable over days and appears independent of exogenous neurotrophin levels or NMDA-receptor signaling.

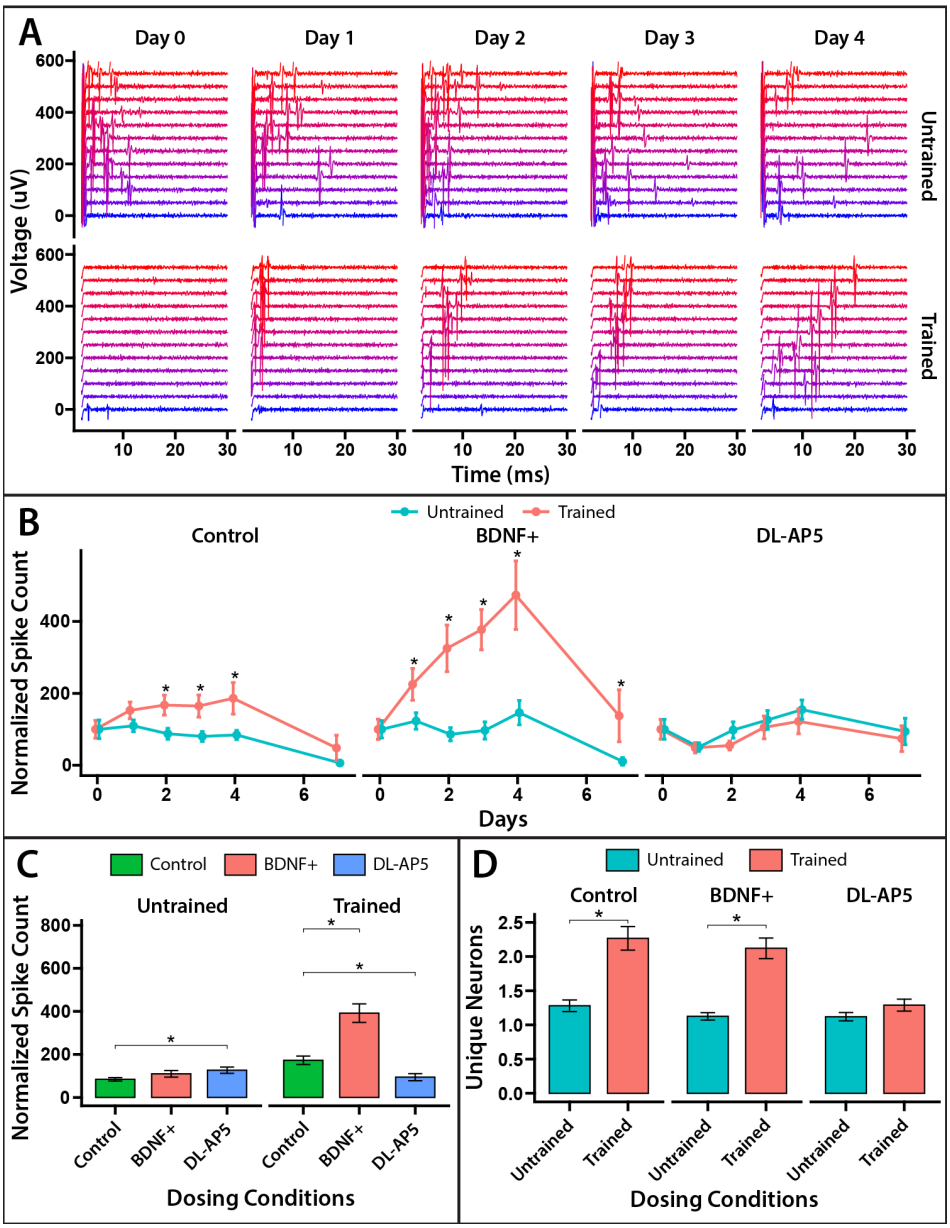

Figure 5. Open-loop stimulation drives long-term potentiation (LTP) that is pharmacologically tunable

A) Spike plots from untrained (top) and trained (bottom) wells illustrate the learning-week trajectory: repeated open-loop stimulation during Evaluation #1 drives a day-by-day increase in evoked network activity in the trained, but not the untrained wells, signaling progressive potentiation. **B)** Population data, expressed as spike counts normalized to Day 0 (mean ± SEM), reveal that the control-medium samples display a significant trained-over-untrained elevation from Day 2 through Day 4. Cultures exposed to 50 ng mL^{-1} BDNF+ potentiate even more rapidly, reaching almost twice the control gain by Day 4, whereas 50 µM DL-AP5 completely abolishes the training effect so that trained and untrained trajectories overlap. **C)** End-of-week (average of days 2-4) comparisons consolidate these findings. Trained cultures maintained in control medium or supplemented with BDNF+ show significantly higher normalized spike counts (mean ± SEM) than those treated with DL-AP5, while the DL-AP5 untrained group unexpectedly exceeds its control counterpart. **D)** End-of-week comparisons of unique neurons (mean ± SEM) identified by spike sorting. The number of unique neurons significantly rises with training in control and BDNF+ media but remains low under NMDA-receptor blockade, consistent with DL-AP5 limiting activity-dependent neuronal recruitment. These results demonstrate a robust, stimulation-driven LTP in CNS-3D organoid networks that can be amplified by exogenous BDNF and suppressed by NMDA-receptor antagonism, establishing the platform's utility for pharmacological interrogation of synaptic plasticity.

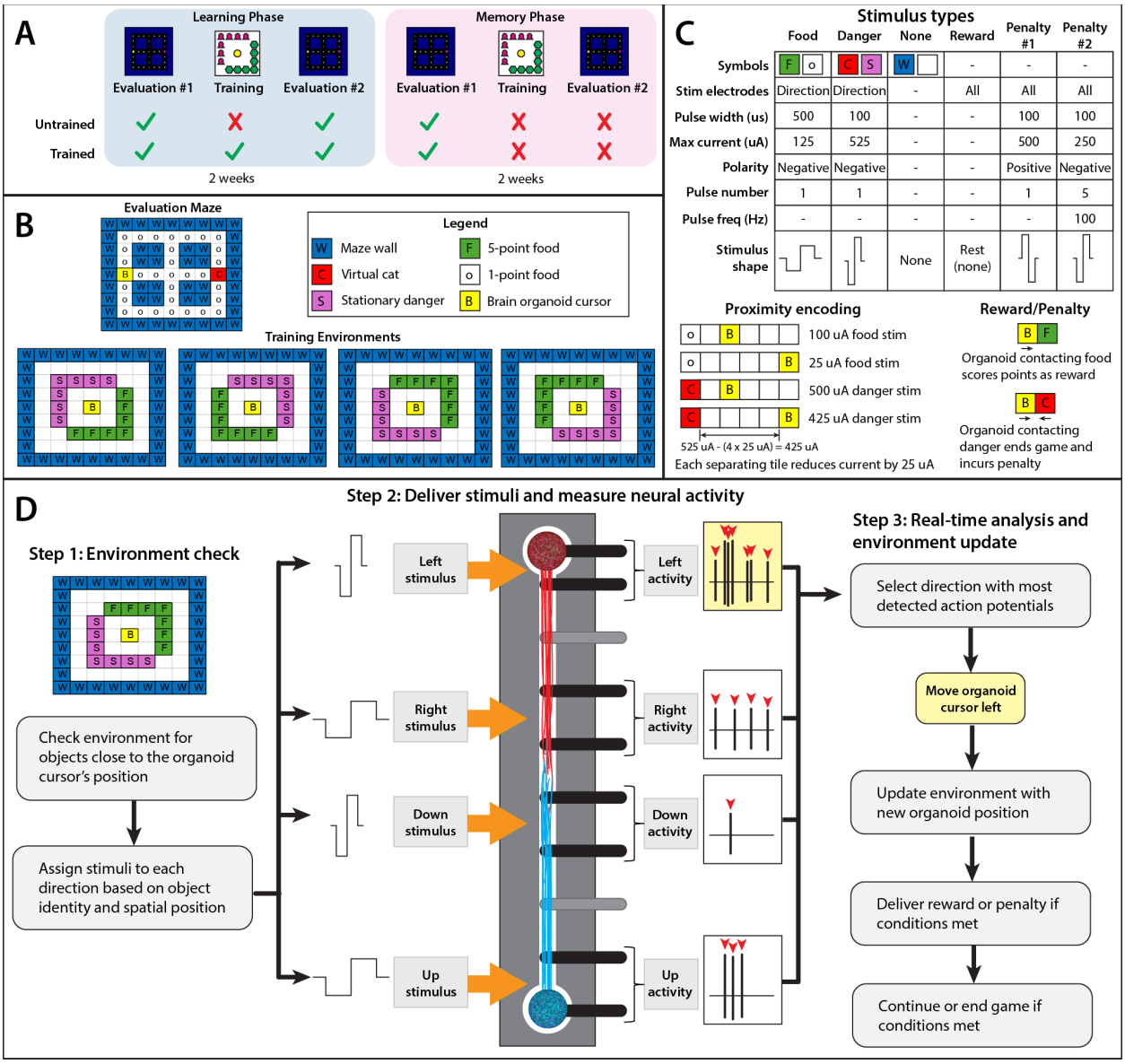

Figure 6. Closed-loop "maze-game" for probing goal-directed learning, memory, and synaptic plasticity in paired brain organoids

A) Experimental schedule. Evaluation #1 (pre-training) consists of three closed-loop maze runs for both untrained and trained cohorts (maximum 60 s per run). The trained cohort then completes a training block: six trials in each of four training mazes (24 total runs, 15 s maximum each). These short mazes repeatedly force the cursor to choose between a food tile (reward stimulus) and a danger tile (penalty stimulus); failure to contact either within 15 s also yields the penalty. The untrained cohort rests during this interval. Finally, Evaluation #2 repeats three runs of the evaluation maze for both cohorts under identical closed-loop conditions, yielding six evaluation trials per cohort in total. **B)** Maze layouts. The single evaluation maze (top left) is used in both Evaluation #1 and #2. Four training mazes (bottom) are rotated permutations of

the same geometry to prevent directional bias. Legend (right) defines tile types used in maze layouts. **C)** Stimulus library. For each tile category - Food, Danger, Background (None), Reward, Penalty-1, Penalty-2 - the accompanying table specifies: addressed electrode pair, biphasic-pulse width, maximum current, polarity, pulse count, pulse frequency, and a schematic waveform. Proximity (lower left) is encoded by amplitude: every grid step between the cursor and a stimulus source reduces stimulus current by 25 µA. The lower right inset illustrates the conditions for scoring a reward versus incurring a penalty. **D)** Closed-loop control cycle. **Step 1:** the controller polls tiles in orthogonal directions (left, right, down, up) and assigns stimulus parameters according to object identity and distance. **Step 2:** biphasic trains are applied simultaneously to the two electrodes that define each direction while multi-unit activity is recorded. **Step 3:** real-time spike counting selects the direction with the highest firing rate, moves the cursor accordingly, updates the virtual environment, and triggers reward or penalty stimuli when conditions are met. A trial terminates on cursor–danger contact or at the time-out limit (training trials also end on food capture). This framework enables direct comparison of learning efficiency, memory retention, and stimulation-dependent modulation of long-term potentiation (LTP) and depression (LTD) between trained and untrained brain-organoid networks.

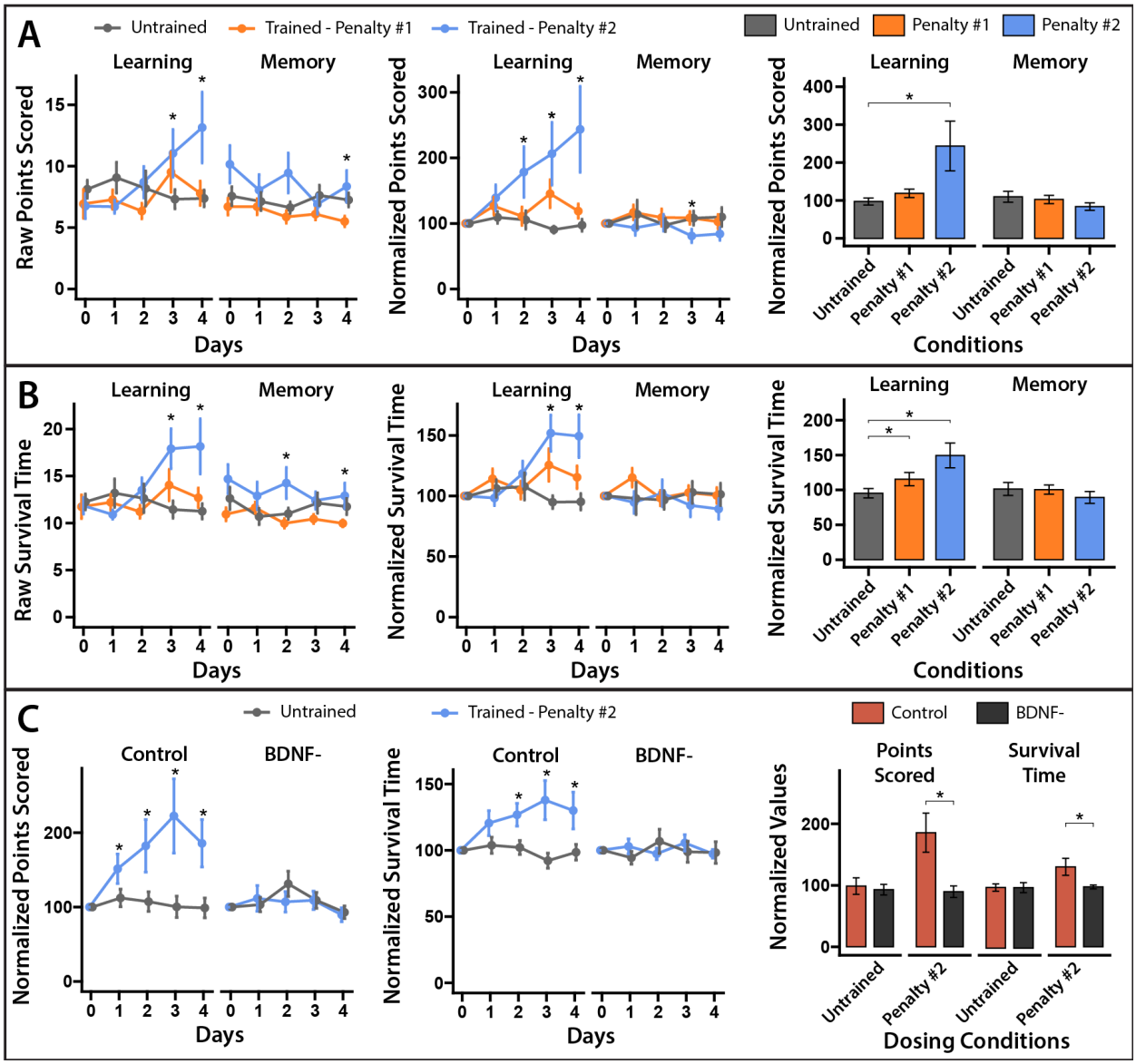

Figure 7. Closed-loop "maze-game" performance reveals penalty-dependent learning and its modulation by BDNF

A) Best-score analysis for the three consecutive maze runs performed each day during Evaluation #1. The left sub-panel plots raw points (mean ± SEM) accumulated during the average learning and memory weeks, revealing overlapping data across groups though Penalty #2 still outperforms the untrained condition. When each sample is normalized to its Day 0 performance (middle sub-panel; mean ± SEM), a clear upward trajectory emerges for cultures trained with Penalty #2 (five-pulse, 100 Hz danger burst) during the average learning week, whereas Penalty #1 (inverted-polarity danger stimulus) remains indistinguishable from untrained controls. The right sub-panel collapses Days 2–4 into an end-of-week mean ± SEM, confirming that only Penalty #2 produces a significant improvement during learning, an effect

that vanishes without reinforcement in the memory phase. **B)** Survival-time outcomes follow a similar pattern. Raw values and their normalized counterparts both show that Penalty #2 lengthens survival progressively during learning; Penalty #1 confers a smaller but still significant benefit, while no group differences persist in memory. Averaged end-of-week data reiterate the superiority of Penalty #2 for extending survival time. **C)** Maze performance depends on exogenous BDNF. In a replication run conducted in control medium containing 20 ng mL^{-1} BDNF, training with Penalty #2 again elevates normalized points and survival time (mean ± SEM) relative to untrained wells. Removing BDNF from the medium abolishes these training-related gains, as shown both in the day-by-day trajectories and in the pooled end-of-week comparisons, indicating that the behavioral advantage conferred by high-frequency penalty bursts requires BDNF signaling. Together, these data demonstrate that a high-frequency burst penalty is more effective than an inverted-polarity penalty at enhancing goal-directed performance and persistence, and that this enhancement is contingent on the presence of BDNF, mirroring the pharmacological modulation observed for long-term potentiation in open-loop experiments.

Acknowledgements

The authors thank Dave Weiner and Alif Saleh (28bio) for their contributions developing and conceptualizing both the open-loop and closed-loop implementations of this work and especially guiding the future applications. The authors would also like to thank Thomas Hartung and Lena Smirnova (Johns Hopkins University) for feedback on experimental design, results, and future directions. We'd also like to thank Alysson Muotri and his lab for the use of the CNS-3D organoid license used in this work.

Methods

Coating Procedure:

For Matrigel coating, an aliquot of Matrigel (Corning, 354277) was placed on ice until mostly thawed, allowing a small piece of ice to remain. Meanwhile, 25 mL of cold DMEM/F12 (50/50) (Corning, 10-092-CV) media was aliquoted into a 50 mL conical tube. A P1000 pipette tip was cooled by aspirating the cold media several times, then approximately 500 µL of the media was left in the tip and added to the Matrigel aliquot. The mixture was gently mixed in the Eppendorf tube to ensure complete thawing, then transferred to the conical containing the cold media. The Eppendorf tube was rinsed twice with portions of the cold media to recover all of the Matrigel. The final coating solution was mixed thoroughly using a serological pipette. Subsequently, 2.5 mL of the matrix solution was added to each 60mm cell culture dish (Cell Treat, 229660), sufficient to coat ten plates. Plates were gently swirled to ensure even coating and then incubated at 37°C for at least one hour or preferably overnight. Plates older than four days were avoided due to potential compromised cell attachment. Prior to use, unbound material was aspirated, and cell suspension or media was added immediately without washing to prevent the surface from drying.

For Laminin coating using Cultrex® Mouse Laminin I (Biotechne, 3400-010-02), the product was thawed at 2–8°C and kept on ice when ready. It was diluted 1:100 in PBS-Ca-Mg (Corning, 21-040-CV) to a concentration of approximately 10 µg/mL and gently homogenized by pipetting. The appropriate volume of the diluted solution was added to each well of the tissue culture plate, ensuring complete coverage of the well bottom. Plates were then incubated at 37°C for four hours or overnight as recommended. When ready for use, the Laminin solution was aspirated, the wells were washed once with PBS-Ca-Mg, and cell suspension was added immediately without allowing the coated surface to dry.

Media Preparation

mTeSRT™1(Stem Cell Technologies, 85850) was prepared by following Stemcell Technologies' Technical Manual Maintenance of Human Pluripotent Stem Cells. Use sterile techniques to

prepare complete mTeSR medium (Basal Medium + 5X Supplement). The following example is for preparing 500 mL of complete medium. The 5X Supplement was thawed to room temperature and mixed thoroughly. If the supplement appeared slightly cloudy, a rare but possible occurrence, it was briefly placed in a 37°C water bath and swirled until clear, for no longer than five minutes. Once fully thawed and clear, 100 mL of the supplement was added to 400 mL of mTeSR Basal Medium and mixed thoroughly without filtering, to avoid loss of essential macromolecules. If not used immediately, the complete medium was stored at 2-8°C for up to two weeks, or aliquoted (40 mL into 50 mL conical tubes) and frozen at -20°C for up to six months. Upon thawing, the medium was used immediately or stored at 2-8°C for up to two weeks, but was never refrozen.

To prepare Neural Basal Complete medium (NBC), 0.5x N2 supplement (Thermo Fischer, 17502-048), 0.5x B27 supplement (Thermo Fischer, 17504-044), and 1x Penicillin-Streptomycin (Hyclone, 16777-164) were added to 500 mL of DMEM/F12 (50/50) containing Glutamine and Hepes. The resulting medium was stable at 4°C for up to one month and protected from light. Aliquots (40 mL) could be frozen in 50 mL conical tubes and stored at -20°C for up to six months. For NBF, a fresh aliquot of bFGF (Thermo Fisher, PHG0023) was thawed on ice and briefly centrifuged. Then, 8 µL of bFGF was added to 40 mL of pre-warmed NB medium (yielding a final concentration of 20 ng/mL) immediately before applying the medium to cells.

To prepare Neural Derivation Medium (NDM), 10 mL of B27 supplement without vitamin A (Thermo Fisher PHG0313), 1x Penicillin-Streptomycin, and 1x Glutamax (Gibco, 35050-061) were added to 500 mL of Neurobasal medium. This medium was also stable at 4°C for one month if shielded from light and could be aliquoted (40 mL per 50 mL tube) and stored at -20°C for up to six months. For NDEF, fresh bFGF and EGF aliquots were thawed on ice, centrifuged briefly, and 8 µL of each was added to 40 mL of pre-warmed ND medium (achieving 20 ng/mL of each factor) before applying it to cells.

Induced Pluripotent Stem Cell (iPSC) Differentiation

iPSCs were differentiated into NPCs as described previously[55,56]. iPSCs colonies were lifted off and kept in suspension, under rotation (95 rpm) for 7 days to form embryoid bodies (EB) in DMEM/F12 50:50 with 1x Glutamax), 1x N2, 1x penicillin-streptomycin, 10-µm SB431542, and 1-µm dorsomorphin.. EBs were gently disrupted, plated onto Matrigel-coated plates, and cultured in DMEM/F12 50:50 with 1x HEPES, 1x Glutamax, 1x PS, 0.5x N2, 0.5x Gem21 NeuroPlex (Gem21; Gemini Bio-products), supplemented with 20-ng/mL basic fibroblast growth factor (bFGF; Life Technologies) and 20ng/mL of epidermal growth factor (EGF; Life Technologies) for 7 days to generate neural rosettes. Neural Rosettes were then manually isolated and enzymatically dissociated into a single-cell suspension. These p1 Neural Progenitor Cells (NPCs) were then expanded up t to create a large working bank for the CNS-3D organoids.

CNS-3D organoid generation from NPCs in 384 well format 3D

NPC's are thawed on a monthly basis to create regular builds of CNS-3D organoids. NPC's are expanded 3 times to then seeded into 384-well low-attachment plates using a BioTek Liquid Handling System, then centrifuged and transferred to a 37°C incubator for culture.

CNS-3D Organoid Maintenance

BrainPhys Complete Media (BPC) was prepared using BrainPhys™ Neuronal Medium with SM1 Kit (StemCell Technologies, 05792) containing 1× penicillin-streptomycin and supplemented with recombinant human brain-derived neurotrophic factor (BDNF) and recombinant human glial cell line-derived neuro-trophic factor (GDNF) (StemCell Technologies; BDNF: Cat# 78005; GDNF: Cat# 78058), each at a final concentration of 20 ng/mL. Each Monday, Wednesday, and Friday organoid cultures received a half media change with the BioTek Liquid Handling System before being placed in the custom, pre coated embedded electrode array (EEA) plate. Organoids were 2, 3, and 5 weeks old before being placed in the EEA plates while optimizing this assay.

EEA Culture Preparation

Custom EEA plates were sterilized and coated with 0.01% Polyethyleneimine (PEI) (Sigma-Aldrich, 181978) in 1X Borate Buffer (Thermo Fisher, 28341) for 1 hour at 37°C temperature. After the incubation period the plates dried for 8 hours and were subsequently coated with 10µg/mL Laminin solution in PBS (Caisson Labs, PBL06) and incubated for minimum 8 hours at 4°C temperature. After coating, the laminin solution was removed. Before seeding the coculture organoids, the plates are equilibrated with 200µL per well of BPC culture media in the 37°C in the incubator.

EEA Culture

Individual organoids were initially transferred from the U-bottom plate into a sterile 100mm petri dish under the BSL2 safety cabinet. The petri dish and lid was transferred to the clean bench where the equilibrated EEA plate was stored. The warmed media was removed, and the organoids were transferred with micro-forceps from the petri dish to the top bulb of the EEA channel and either the 3rd or 4th bulb (2mm and 4mm down the channel) using micro-forceps (Dumostar, 11294) with a microscope in a Thermo Fisher-Scientific Heraguard Eco Clean bench. Eventually, 4mm was the decided positioning. The organoids were covered with 200 µL of BPC media and returned to the incubator. The organoids adhered for 3 days undisturbed in the incubator; on day 3 the entirety of the channel was covered in Matrigel (Corning, 354230) to allow for 3D growth over the electrodes. The matrigel was placed by removing the cultures from

the incubator and placing it in the clean bench. Culture media was removed with a pipette to expose the channel. 2-3µL of Matrigel was dispensed into the channel, filling and covering the entirety of the channel and bulbs. After 2-3 minutes, once the matrigel was hardened 200µL of fresh BPC media was dispensed into each well. After this matrigel procedure and media change, a regular Monday, Wednesday, Friday full 200µL media change was established for the following 2-7 weeks. Weekly imaging was performed during the growth weeks to ensure PNS-3D organoid cultures were healthy and robust before dosing took place.

Imaging methods

Organoid images were taken on the Molecular Devices ImageXpress Micro Confocal Microscope on DIV 4 of the organoid formation phase before organoids were placed in the bulb of the EEA channel to ensure all organoids had formed correctly. The TL25 images were taken with a 4X objective with a 0.05ms exposure time. Weekly imaging was performed once per week to ensure the health and growth of the cultures. Cultures were imaged with the Molecular Devices ImageXpress Micro Confocal Microscope in TL25, with a 10X objective for 7.27ms exposure. Z planes of 19 steps across 8 sites down the channel allowed us to visualize the 3D nature of the peripheral nerve. The range was 15µm between steps for a total range of 270µm. During the dosing week, cell cultures were imaged 2 additional times, once in the middle of the week and once at the end of the seven-day dose period. Images were stitched together with a custom Matlab application for growth analysis and monitoring.

Dosing

After two weeks of EEA culture, organoids underwent 2 weeks of compound testing for the remainder of culture. For the LTP study cultures underwent full media changes every Monday, Wednesday and Friday with 200µM DL-APV (Medchem Express, HY-100714) in Brainphys Complete Media, 50ng/mL BDNF in Brainphys Complete Media, and control media. For the maze study, 50ng/mL BDNF in Brainphys Complete Media, Brainphys Complete media without BDNF, and control media were applied in the same manner but for four weeks while undergoing electrophysiological training and assessment.

Stimulation and Recording Methods

All electrophysiology experiments were conducted using a custom 24-well embedded electrode array (EEA) plate that allows concurrent stimulation and recording from paired organoids. Each well contained ten planar microelectrodes (50 µm diameter) embedded in the floor of the inter-organoid channel, along with integrated reference electrodes at each end of the channel (1.2 mm diameter) to provide a common ground. Custom headstages incorporating Intan RHS2116 stimulator/amplifier chips (Intan Technologies) were used to interface the EEA plate with the recording hardware. Two data acquisition systems were utilized: an Intan RHS Stim/Recording Controller running RHX v3.1.0 software, and an Alpha Omega AlphaRS Pro

system running AlphaRS proprietary software. The Intan RHS system is a 128-channel-count system interfaced with a custom headstage allowing 12 of 24 wells to be stimulated/recorded simultaneously in open-loop configuration. The AlphaRS Pro is a 256-channel-count system capable of simultaneous stimulation/recording of all 24 wells using a custom headstage in both open-loop and real-time closed-loop control. Signals from the RHS2116-based headstages were digitized at 30 kHz and band-pass filtered (analog passband 80–7500 Hz) on-board to capture action potentials. During stimulation, the Intan amplifiers engaged an artifact suppression mode by temporarily reducing the high-pass cutoff to ~1 kHz to minimize stimulus artifacts. Recorded data were saved in Intan's RHX format (.rhd) or a MATLAB-based format on the AlphaRS system. All stimulation used current-controlled, biphasic pulses with phase durations matched and opposite in polarity to ensure charge balance. Each electrode could serve for both recording and stimulation, with the stimulus waveform routed through the RHS2116 stimulator channels under software control. The stimulation and recording protocols were implemented in two modes: open-loop and closed-loop (Figure 1C). In open-loop experiments, predefined stimulation patterns were delivered to the organoids while neural responses were recorded, without any real-time feedback. In closed-loop experiments, stimulation parameters were dynamically adjusted based on the organoid network's ongoing activity (see Closed-Loop Maze Paradigm below).

Open-Loop Stimulation

Open-loop stimulation protocols were designed to probe and induce synaptic plasticity. We systematically explored a range of stimulus parameters to optimize evoked responses. This included varying the pulse amplitude (e.g. 25–400 µA), pulse width (100–500 µs per phase), number of pulses in a train (single pulse vs. short high-frequency bursts of 5 or 10 pulses), pulse frequency (e.g. 50 Hz or 100 Hz for bursts), and pulse polarity (standard cathodic-first vs. inverted polarity anodic-first for certain aversive stimuli). Each stimulation "trial" consisted of delivering a specific pulse or pulse train on one or more electrodes and recording the post-stimulus response. A custom MATLAB 2024a application orchestrated all stimulus delivery and data acquisition. Stimulation protocols were defined in a spreadsheet script (Excel format) listing the sequence of stimulus parameters (electrode selection, current amplitude, pulse width, polarity, number of pulses, and trial timing). The MATLAB controller interfaced with the Intan RHX software via TCP/IP or with the AlphaRS Pro API to load each stimulus configuration and trigger synchronized stimulation/recording in the hardware. This setup enabled rapid switching between different stimulus conditions and automated execution of complex stimulation paradigms across the 24-well plate. Parameter tuning experiments (see Results, Fig. 3D) were conducted in open-loop mode to identify stimulus settings that elicited reliable spiking (multi-unit) responses from the organoid networks. Unless otherwise noted, all stimuli were delivered as biphasic pulses with 0.1 ms inter-phase intervals, and trials were separated by

at least 1 s to allow network recovery. For plasticity induction (LTP/LTD) studies, repetitive stimulation trains were delivered over several days as described later, with control (unstimulated) organoids maintained in parallel for comparison.

Closed-Loop Maze Paradigm

For closed-loop experiments, we developed an interactive "maze game" paradigm to provide real-time feedback-driven stimulation. The closed-loop system linked the organoid electrophysiology to a virtual agent navigating a grid-based maze, using principles of reinforcement learning to emulate goal-directed behavior. The game environment was implemented in MATLAB and presented four cardinal directions (up, down, left, right) as possible moves for the agent. In each closed-loop trial, an organoid pair was tasked with guiding the agent from a start location to a target ("food") while avoiding danger. Custom logic translated neural activity into directional decisions and delivered feedback stimuli based on the agent's progress.

Each maze was composed of a 2D grid of tiles with designated properties (open path, food, danger, etc.), as illustrated in Fig. 6B. We utilized two types of mazes: evaluation mazes and training mazes. Evaluation mazes (used in pre- and post-training assessments) had a fixed layout with one food target and a computer-controlled pursuer (obstacle) to challenge the organoid without any additional training cues. Training mazes were simpler configurations that required a binary choice (turn toward food vs. toward danger), and we employed four rotational variants of a basic two-choice maze. This ensured that across trials each cardinal direction was equally likely to be "correct," preventing any directional bias in the organoids' responses. Organoid pairs underwent daily training sessions in which they experienced a series of these maze trials with feedback, followed later by evaluation trials without feedback to test learned performance. A typical training session consisted of multiple maze runs (e.g. 10–20 trials per day), and training was carried out over 5–7 days (constituting the "learning phase"). In the subsequent week (the "memory phase"), the organoids were tested in evaluation mazes without further feedback to assess retention of any learned behavior. Performance metrics recorded included the total points (rewards) earned per trial and the survival time (time until hitting danger), which were averaged or summed over sets of trials for comparison across days.

The neural interface between the organoids and the maze game operated on a cycle of stimulate-listen-act that repeated continuously during each trial. At each time step (iteration) of the game, the system delivered four *directional stimuli* simultaneously: one cue for each cardinal direction. These stimuli were delivered through four distinct pairs of electrodes on the EEA (each pair corresponding to one direction), targeting different spatial regions of the organoid network. For example, "up" stimuli might be delivered on a pair of electrodes located under the top organoid, whereas "down" stimuli target electrodes under the bottom organoid,

and “left”/“right” stimuli delivered in the connecting channel or opposing sides, such that each direction had a unique spatial stimulation pattern. All directional cues were biphasic pulses with moderate current (outlined in Fig. 6C) delivered concurrently. The stimulation parameters for each cue were optimized to be salient but not evoking overwhelming activity, so that the organoids’ differential response could indicate a “preference.” Immediately after delivering the directional cues, the system entered a listening period (~100 ms) during which multi-unit firing activity from the organoids was recorded in real time. A fast online analysis computed the firing rate on each of the four directional electrode pairs (using threshold crossing to detect spikes). The direction yielding the highest summed spike rate was interpreted as the organoids’ choice for that step. Consequently, the virtual agent was moved one tile in that chosen direction. This closed-loop decision process effectively allowed the organoid network’s activity to control the agent’s navigation: the organoids “steered” the agent by generating more spikes in response to one of the directional stimuli.

As the agent moved through the maze, context-specific feedback stimuli were provided to reinforce learning. We designed a library of unique electrical stimuli mapped to important game events. For instance, when the agent’s next move would place it adjacent to the food target, a special “food proximity” stimulus was delivered on the electrodes oriented toward the food’s location. This cue consisted of a single cathodic-first, 500 us-100 uA pulse, meant to signal that the goal is near. Likewise, approaching a dangerous tile triggered a “danger proximity” stimulus on the electrodes facing that direction, alerting the organoid of impending penalty. If the agent successfully reached the food tile, a reward stimulus was issued: rather than an electrical pulse, the reward was a 1–2 s pause in stimulation (no stimuli delivered). This lack-of-stimulus period served as a positive reinforcement, under the assumption that whatever neural activity led to the success would be intrinsically strengthened by a brief cessation of perturbation. In contrast, if the agent stepped onto a danger tile, a penalty stimulus was delivered to induce negative reinforcement. We tested two different penalty configurations. Penalty #1 was a single biphasic pulse of inverted polarity (anodic-first) at a relatively high current, intended to be an aversive signal. Penalty #2 was a stronger stimulus: a burst of five high-frequency pulses (e.g. 5 pulses at 100 Hz, cathodic-first) at the 250 uA. Both penalty types were delivered on a broad set of electrodes spanning both organoids and the mid-channel, to engage a large portion of the network. To incorporate spatial information, we modulated stimulus intensity based on the agent’s distance from the target or danger. Specifically, for every grid step further away from the food or danger, the amplitude of the proximity stimuli was linearly decreased by 25 µA (for example, if 75 µA at 1 step away, then 50 µA at 2 steps, 25 µA at 3 steps, etc.). This created a gradient of stimulus strength that the organoids could potentially sense, analogous to sensing a gradient in chemical or sensory cues. Throughout closed-loop operation, the MATLAB control program handled real-time event detection and stimulation with a loop cycle on the order of

tens of milliseconds, ensuring low latency feedback. Trial outcomes (success or failure), points earned, and survival time were logged for each run. These performance metrics were later used to quantify learning by comparing the trained organoids' improvements against untrained controls and across different feedback strategies.

Data Analysis

Recorded electrophysiological data were analyzed both offline (for open-loop experiments) and online (for closed-loop experiments), using custom scripts in MATLAB and R. Preprocessing of raw voltage traces included artifact removal and spike detection. For open-loop stimulus-response data, each trial's recording was segmented from –100 ms to +500 ms relative to stimulus onset, using the recorded trigger timestamps. A baseline correction was applied to remove stimulus artifacts: we subtracted a copy of the signal low-pass filtered at 10 Hz (4th-order Butterworth, zero-phase) from the raw trace, effectively eliminating slow drift and residual stimulus offset without distorting fast action potentials. The preprocessed trial matrices were then used to compute quantitative metrics of evoked activity. We detected action potentials (spikes) in the high-pass filtered data using an amplitude threshold set at ~4–5× the noise standard deviation. Detected spike waveforms were aligned to their trough and then subjected to spike sorting to distinguish putative single neurons. We employed feature-based clustering methods using a wavelet-transform clustering algorithm (adapted from Quian Quiroga et al. 2004) to automatically group spikes into units[41]. Each sorted unit's spike train was examined across the recording period to ensure stability of waveform shape and firing characteristics. For quality control, units with refractory period violations or unstable waveforms were excluded from single-unit analyses, and the remaining multi-unit activity (including all threshold crossings) was used for overall network activity measures.

Burst analysis

Burst analysis of spontaneous activity was performed to characterize network oscillations and plasticity. We defined a network burst as a sequence of at least 3 spikes with short inter-spike intervals, using a maximum interval method. Specifically, any spikes occurring with consecutive inter-spike intervals ≤ 170 ms were grouped into a burst, as long as the burst duration exceeded 10 ms and the burst was separated from the next spike by at least 200 ms (minimum inter-burst interval). This algorithm was applied to spike timestamps on each electrode (or each sorted unit), yielding burst onset times and burst durations for each recording. From these, we computed the burst frequency (bursts per minute) and mean spikes per burst for each condition. To visualize changes in bursting over time, we employed kernel density estimation (KDE): burst event timestamps were convolved with a Gaussian kernel (bandwidth on the order of the burst interval) to obtain a continuous estimate of burst rate as a function of time. For example, in assessing the development of connectivity between organoids, we compared the

KDE of burst frequency on electrodes under each organoid vs. those in the middle of the channel over the first few weeks of co-culture (see Fig. 3B), which illustrated the emergence of synchronized bursting as axonal connections formed.

Evoked response analysis

Evoked response analysis for plasticity experiments focused on quantifying changes in spike output due to training. For each organoid pair, we measured the number of spikes (or multi-unit firing rate) in a 0–300 ms window after each stimulus, and in some cases the integrated voltage envelope of the response, to capture subthreshold contributions. Potentiation was evaluated by comparing these metrics before and after the training protocol. For short-term potentiation experiments, we normalized evoked response magnitudes to each sample's own baseline (pre-training on the same day) value to calculate % change due to training. For long-term potentiation experiments, we instead normalized evoked response magnitudes to each sample's own baseline at the beginning of each week to calculate % change over time. Similarly, for closed-loop behavioral experiments, performance metrics (total points and survival time) were normalized to each organoid pair's initial baseline run at the beginning of each week to account for individual differences.

Statistical analyses

Statistical analyses were carried out to determine the significance of observed changes. Depending on the comparison, we used unpaired two-tailed t-tests for single variable comparisons or repeated-measures ANOVA for multi-day learning trends, with post hoc tests (Tukey's HSD) for multiple comparisons. Non-parametric alternatives (Wilcoxon signed-rank or rank-sum tests) were used if data violated normality assumptions. Data are generally reported as mean ± standard error of the mean (SEM). A significance threshold of $p < 0.05$ was applied for all tests. To assess pharmacological effects, two-factor analyses were used (treatment × training) to test for interaction effects (e.g., whether NMDA receptor blockade by AP5 influenced the degree of LTP induced, or whether BDNF withdrawal affected learning outcomes). All analyses were implemented in MATLAB R2024a or R (v4.3) using custom-written scripts and built-in statistical libraries.

Visualization

Visualization of results was done using MATLAB and R (ggplot2), with kernel density plots for firing rate/burst distributions, line and bar graphs for time-course and group comparisons, and scatter plots for single-unit activity metrics. Figures were assembled in Adobe Illustrator, with schematics of the experimental setup created in-house to illustrate the EEA platform and neural interface overview. Each dataset was reviewed for outliers or technical artifacts, and any exclusions are noted in the Results. Together, these data analysis methods enabled us to

quantify synaptic potentiation and learning-related changes in the organoid cultures with rigor and reproducibility.

References

(1) Gribkoff, V. K.; Kaczmarek, L. K. The Need for New Approaches in CNS Drug Discovery: Why Drugs Have Failed, and What Can Be Done to Improve Outcomes. *Neuropharmacology* **2017**, *120*, 11–19. https://doi.org/10.1016/j.neuropharm.2016.03.021.

(2) Vatansever, S.; Schlessinger, A.; Wacker, D.; Kaniskan, H. Ü.; Jin, J.; Zhou, M.-M.; Zhang, B. Artificial Intelligence and Machine Learning-Aided Drug Discovery in Central Nervous System Diseases: State-of-the-Arts and Future Directions. *Medicinal Research Reviews* **2021**, *41* (3), 1427–1473. https://doi.org/10.1002/med.21764.

(3) Pradeepkiran, J. A.; Baig, J.; Islam, M. A.; Kshirsagar, S.; Reddy, P. H. Amyloid-β and Phosphorylated Tau Are the Key Biomarkers and Predictors of Alzheimer's Disease. *Aging Dis* **2024**, *16* (2), 658–682. https://doi.org/10.14336/AD.2024.0286.

(4) Jack Jr., C. R.; Bennett, D. A.; Blennow, K.; Carrillo, M. C.; Dunn, B.; Haeberlein, S. B.; Holtzman, D. M.; Jagust, W.; Jessen, F.; Karlawish, J.; Liu, E.; Molinuevo, J. L.; Montine, T.; Phelps, C.; Rankin, K. P.; Rowe, C. C.; Scheltens, P.; Siemers, E.; Snyder, H. M.; Sperling, R.; Contributors; Elliott, C.; Masliah, E.; Ryan, L.; Silverberg, N. NIA-AA Research Framework: Toward a Biological Definition of Alzheimer's Disease. *Alzheimer's & Dementia* **2018**, *14* (4), 535–562. https://doi.org/10.1016/j.jalz.2018.02.018.

(5) Zhang, Y.; Chen, H.; Li, R.; Sterling, K.; Song, W. Amyloid β-Based Therapy for Alzheimer's Disease: Challenges, Successes and Future. *Sig Transduct Target Ther* **2023**, *8* (1), 248. https://doi.org/10.1038/s41392-023-01484-7.

(6) Citri, A.; Malenka, R. C. Synaptic Plasticity: Multiple Forms, Functions, and Mechanisms. *Neuropsychopharmacol* **2008**, *33* (1), 18–41. https://doi.org/10.1038/sj.npp.1301559.

(7) Morris, R. G.; Anderson, E.; Lynch, G. S.; Baudry, M. Selective Impairment of Learning and Blockade of Long-Term Potentiation by an N-Methyl-D-Aspartate Receptor Antagonist, AP5. *Nature* **1986**, *319* (6056), 774–776. https://doi.org/10.1038/319774a0.

(8) Koffie, R. M.; Hyman, B. T.; Spires-Jones, T. L. Alzheimer's Disease: Synapses Gone Cold. *Mol Neurodegener* **2011**, *6* (1), 63. https://doi.org/10.1186/1750-1326-6-63.

(9) Wu, X.-L.; Yan, Q.-J.; Zhu, F. Abnormal Synaptic Plasticity and Impaired Cognition in Schizophrenia. *World J Psychiatry* **2022**, *12* (4), 541–557. https://doi.org/10.5498/wjp.v12.i4.541.

(10) Teyler, T. J. Use of Brain Slices to Study Long-Term Potentiation and Depression as Examples of Synaptic Plasticity. *Methods* **1999**, *18* (2), 109–116. https://doi.org/10.1006/meth.1999.0764.

(11) Chen, W. R.; Lee, S.; Kato, K.; Spencer, D. D.; Shepherd, G. M.; Williamson, A. Long-Term Modifications of Synaptic Efficacy in the Human Inferior and Middle Temporal Cortex. *Proc Natl Acad Sci U S A* **1996**, *93* (15), 8011–8015. https://doi.org/10.1073/pnas.93.15.8011.

(12) El Din, D.-M. A.; Moenkemoeller, L.; Loeffler, A.; Habibollahi, F.; Schenkman, J.; Mitra, A.; van der Molen, T.; Ding, L.; Laird, J.; Schenke, M.; Johnson, E. C.; Kagan, B. J.; Hartung, T.;

Smirnova, L. Human Neural Organoid Microphysiological Systems Show the Building Blocks Necessary for Basic Learning and Memory. *bioRxiv* **2024**, 2024.09.17.613333. https://doi.org/10.1101/2024.09.17.613333.

(13) Lancaster, M. A.; Renner, M.; Martin, C.-A.; Wenzel, D.; Bicknell, L. S.; Hurles, M. E.; Homfray, T.; Penninger, J. M.; Jackson, A. P.; Knoblich, J. A. Cerebral Organoids Model Human Brain Development and Microcephaly. *Nature* **2013**, *501* (7467), 373–379. https://doi.org/10.1038/nature12517.

(14) Trujillo, C. A.; Muotri, A. R. Brain Organoids and the Study of Neurodevelopment. *Trends Mol Med* **2018**, *24* (12), 982–990. https://doi.org/10.1016/j.molmed.2018.09.005.

(15) Pamies, D.; Barrera, P.; Block, K.; Makri, G.; Kumar, A.; Wiersma, D.; Smirnova, L.; Zhang, C.; Bressler, J.; Christian, K. M.; Harris, G.; Ming, G.; Berlinicke, C. J.; Kyro, K.; Song, H.; Pardo, C. A.; Hartung, T.; Hogberg, H. T. A Human Brain Microphysiological System Derived from Induced Pluripotent Stem Cells to Study Neurological Diseases and Toxicity. *ALTEX* **2017**, *34* (3), 362–376. https://doi.org/10.14573/altex.1609122.

(16) Chesnut, M.; Hartung, T.; Hogberg, H.; Pamies, D. Human Oligodendrocytes and Myelin In Vitro to Evaluate Developmental Neurotoxicity. *Int J Mol Sci* **2021**, *22* (15), 7929. https://doi.org/10.3390/ijms22157929.

(17) Trujillo, C. A.; Gao, R.; Negraes, P. D.; Gu, J.; Buchanan, J.; Preissl, S.; Wang, A.; Wu, W.; Haddad, G. G.; Chaim, I. A.; Domissy, A.; Vandenberghe, M.; Devor, A.; Yeo, G. W.; Voytek, B.; Muotri, A. R. Complex Oscillatory Waves Emerging from Cortical Organoids Model Early Human Brain Network Development. *Cell Stem Cell* **2019**, *25* (4), 558-569.e7. https://doi.org/10.1016/j.stem.2019.08.002.

(18) Wang, Q.; Cohen, J. D.; Yukawa, T.; Estrella, H.; Leonard, C.; Nunes, J.; Choi, C.; Lewis, L.; Baker, K. S.; Kuga, K.; Dragan, Y. P.; Wagoner, M. P.; Mishra, N. Assessment of a 3D Neural Spheroid Model to Detect Pharmaceutical-Induced Neurotoxicity. *ALTEX* **2022**, *39* (4), 560–582. https://doi.org/10.14573/altex.2112221.

(19) Yanakiev, M.; Soper, O.; Berg, D. A.; Kang, E. Modelling Alzheimer's Disease Using Human Brain Organoids: Current Progress and Challenges. *Expert Reviews in Molecular Medicine* **2023**, *25*, e3. https://doi.org/10.1017/erm.2022.40.

(20) Kim, H.; Park, H. J.; Choi, H.; Chang, Y.; Park, H.; Shin, J.; Kim, J.; Lengner, C. J.; Lee, Y. K.; Kim, J. Modeling G2019S-LRRK2 Sporadic Parkinson's Disease in 3D Midbrain Organoids. *Stem Cell Reports* **2019**, *12* (3), 518–531. https://doi.org/10.1016/j.stemcr.2019.01.020.

(21) Shoemaker, A. R.; Jones, I. E.; Jeffris, K. D.; Gabrielli, G.; Togliatti, A. G.; Pichika, R.; Martin, E.; Kiskinis, E.; Franz, C. K.; Finan, J. D. Biofidelic Dynamic Compression of Human Cortical Spheroids Reproduces Neurotrauma Phenotypes. *Dis Model Mech* **2021**, *14* (12), dmm048916. https://doi.org/10.1242/dmm.048916.

(22) Urresti, J.; Zhang, P.; Moran-Losada, P.; Yu, N.-K.; Negraes, P. D.; Trujillo, C. A.; Antaki, D.; Amar, M.; Chau, K.; Pramod, A. B.; Diedrich, J.; Tejwani, L.; Romero, S.; Sebat, J.; Yates Iii, J. R.; Muotri, A. R.; Iakoucheva, L. M. Cortical Organoids Model Early Brain Development Disrupted by 16p11.2 Copy Number Variants in Autism. *Mol Psychiatry* **2021**, *26* (12), 7560–7580. https://doi.org/10.1038/s41380-021-01243-6.

(23) Marchetto, M. C. N.; Carromeu, C.; Acab, A.; Yu, D.; Yeo, G. W.; Mu, Y.; Chen, G.; Gage, F. H.; Muotri, A. R. A Model for Neural Development and Treatment of Rett Syndrome Using

Human Induced Pluripotent Stem Cells. *Cell* **2010**, *143* (4), 527–539. https://doi.org/10.1016/j.cell.2010.10.016.

(24) Tang, X.; Kim, J.; Zhou, L.; Wengert, E.; Zhang, L.; Wu, Z.; Carromeu, C.; Muotri, A. R.; Marchetto, M. C. N.; Gage, F. H.; Chen, G. KCC2 Rescues Functional Deficits in Human Neurons Derived from Patients with Rett Syndrome. *Proc Natl Acad Sci U S A* **2016**, *113* (3), 751–756. https://doi.org/10.1073/pnas.1524013113.

(25) Negraes, P. D.; Trujillo, C. A.; Yu, N.-K.; Wu, W.; Yao, H.; Liang, N.; Lautz, J. D.; Kwok, E.; McClatchy, D.; Diedrich, J.; de Bartolome, S. M.; Truong, J.; Szeto, R.; Tran, T.; Herai, R. H.; Smith, S. E. P.; Haddad, G. G.; Yates, J. R.; Muotri, A. R. Altered Network and Rescue of Human Neurons Derived from Individuals with Early-Onset Genetic Epilepsy. *Mol Psychiatry* **2021**, *26* (11), 7047–7068. https://doi.org/10.1038/s41380-021-01104-2.

(26) Zafeiriou, M.-P.; Bao, G.; Hudson, J.; Halder, R.; Blenkle, A.; Schreiber, M.-K.; Fischer, A.; Schild, D.; Zimmermann, W.-H. Developmental GABA Polarity Switch and Neuronal Plasticity in Bioengineered Neuronal Organoids. *Nat Commun* **2020**, *11* (1), 3791. https://doi.org/10.1038/s41467-020-17521-w.

(27) Osaki, T.; Duenki, T.; Chow, S. Y. A.; Ikegami, Y.; Beaubois, R.; Levi, T.; Nakagawa-Tamagawa, N.; Hirano, Y.; Ikeuchi, Y. Complex Activity and Short-Term Plasticity of Human Cerebral Organoids Reciprocally Connected with Axons. *Nat Commun* **2024**, *15* (1), 2945. https://doi.org/10.1038/s41467-024-46787-7.

(28) Robbins, A.; Schweiger, H. E.; Hernandez, S.; Spaeth, A.; Voitiuk, K.; Parks, D. F.; van der Molen, T.; Geng, J.; Sharf, T.; Mostajo-Radji, M. A.; Haussler, D.; Teodorescu, M. Goal-Directed Learning in Cortical Organoids. *bioRxiv* **2024**, 2024.12.07.627350. https://doi.org/10.1101/2024.12.07.627350.

(29) Smirnova, L.; Caffo, B. S.; Gracias, D. H.; Huang, Q.; Morales Pantoja, I. E.; Tang, B.; Zack, D. J.; Berlinicke, C. A.; Boyd, J. L.; Harris, T. D.; Johnson, E. C.; Kagan, B. J.; Kahn, J.; Muotri, A. R.; Paulhamus, B. L.; Schwamborn, J. C.; Plotkin, J.; Szalay, A. S.; Vogelstein, J. T.; Worley, P. F.; Hartung, T. Organoid Intelligence (OI): The New Frontier in Biocomputing and Intelligence-in-a-Dish. *Front. Sci.* **2023**, *1*. https://doi.org/10.3389/fsci.2023.1017235.

(30) Wadan, A.-H. S. Organoid Intelligence and Biocomputing Advances: Current Steps and Future Directions. *Brain Organoid and Systems Neuroscience Journal* **2025**, *3*, 8–14. https://doi.org/10.1016/j.bosn.2025.01.002.

(31) Kagan, B. J.; Kitchen, A. C.; Tran, N. T.; Habibollahi, F.; Khajehnejad, M.; Parker, B. J.; Bhat, A.; Rollo, B.; Razi, A.; Friston, K. J. *In Vitro* Neurons Learn and Exhibit Sentience When Embodied in a Simulated Game-World. *Neuron* **2022**, *110* (23), 3952-3969.e8. https://doi.org/10.1016/j.neuron.2022.09.001.

(32) Morales Pantoja, I. E.; Smirnova, L.; Muotri, A. R.; Wahlin, K. J.; Kahn, J.; Boyd, J. L.; Gracias, D. H.; Harris, T. D.; Cohen-Karni, T.; Caffo, B. S.; Szalay, A. S.; Han, F.; Zack, D. J.; Etienne-Cummings, R.; Akwaboah, A.; Romero, J. C.; Alam El Din, D.-M.; Plotkin, J. D.; Paulhamus, B. L.; Johnson, E. C.; Gilbert, F.; Curley, J. L.; Cappiello, B.; Schwamborn, J. C.; Hill, E. J.; Roach, P.; Tornero, D.; Krall, C.; Parri, R.; Sillé, F.; Levchenko, A.; Jabbour, R. E.; Kagan, B. J.; Berlinicke, C. A.; Huang, Q.; Maertens, A.; Herrmann, K.; Tsaioun, K.; Dastgheyb, R.; Habela, C. W.; Vogelstein, J. T.; Hartung, T. First Organoid Intelligence (OI) Workshop to Form an OI Community. *Front. Artif. Intell.* **2023**, *6*. https://doi.org/10.3389/frai.2023.1116870.

(33) Nathan, P. J.; Cobb, S. R.; Lu, B.; Bullmore, E. T.; Davies, C. H. Studying Synaptic Plasticity in the Human Brain and Opportunities for Drug Discovery. *Current Opinion in Pharmacology* **2011**, *11* (5), 540–548. https://doi.org/10.1016/j.coph.2011.06.008.
(34) Anderson, W. A.; Bosak, A.; Hogberg, H. T.; Hartung, T.; Moore, M. J. Advances in 3D Neuronal Microphysiological Systems: Towards a Functional Nervous System on a Chip. *In Vitro Cell.Dev.Biol.-Animal* **2021**, *57* (2), 191–206. https://doi.org/10.1007/s11626-020-00532-8.
(35) Onesto, M. M.; Kim, J.; Pasca, S. P. Assembloid Models of Cell-Cell Interaction to Study Tissue and Disease Biology. *Cell Stem Cell* **2024**, *31* (11), 1563–1573. https://doi.org/10.1016/j.stem.2024.09.017.
(36) Wu, S.-R.; Nowakowski, T. J. Exploring Human Brain Development and Disease Using Assembloids. *Neuron* **2025**, *113* (8), 1133–1150. https://doi.org/10.1016/j.neuron.2025.02.010.
(37) Pollard, K. J.; Bowser, D. A.; Anderson, W. A.; Meselhe, M.; Moore, M. J. Morphine-Sensitive Synaptic Transmission Emerges in Embryonic Rat Microphysiological Model of Lower Afferent Nociceptive Signaling. *Sci Adv* **2021**, *7* (35), eabj2899. https://doi.org/10.1126/sciadv.abj2899.
(38) Rountree, C.; Rodriguez, T.; Byrne, E.; Schmidt, E.; Schwarzbach, E.; Dillon, S.; McCrimmon, A.; Terral, M.; Metea, M.; Moore, M. J.; Curley, J. L. Human Peripheral Nerve-on-a-Chip on a Multiwell Microelectrode Array as a Scalable Preclinical Neurotoxicity Assay. bioRxiv June 23, 2025, p 2025.06.09.658615. https://doi.org/10.1101/2025.06.09.658615.
(39) Imredy, J. P.; Roussignol, G.; Clouse, H.; Salvagiotto, G.; Mazelin-Winum, L. Comparative Assessment of Ca2+ Oscillations in 2- and 3-Dimensional hiPSC Derived and Isolated Cortical Neuronal Networks. *Journal of Pharmacological and Toxicological Methods* **2023**, *123*, 107281. https://doi.org/10.1016/j.vascn.2023.107281.
(40) Lafon, B.; Rahman, A.; Bikson, M.; Parra, L. C. Direct Current Stimulation Alters Neuronal Input/Output Function. *Brain Stimul* **2017**, *10* (1), 36–45. https://doi.org/10.1016/j.brs.2016.08.014.
(41) Quiroga, R. Q.; Nadasdy, Z.; Ben-Shaul, Y. Unsupervised Spike Detection and Sorting with Wavelets and Superparamagnetic Clustering. *Neural Comput* **2004**, *16* (8), 1661–1687. https://doi.org/10.1162/089976604774201631.
(42) Miao, H.-H.; Miao, Z.; Pan, J.-G.; Li, X.-H.; Zhuo, M. Brain-Derived Neurotrophic Factor Produced Long-Term Synaptic Enhancement in the Anterior Cingulate Cortex of Adult Mice. *Molecular Brain* **2021**, *14* (1), 140. https://doi.org/10.1186/s13041-021-00853-z.
(43) Bliss, T. V.; Lomo, T. Long-Lasting Potentiation of Synaptic Transmission in the Dentate Area of the Anaesthetized Rabbit Following Stimulation of the Perforant Path. *J Physiol* **1973**, *232* (2), 331–356. https://doi.org/10.1113/jphysiol.1973.sp010273.
(44) Ying, S.-W.; Futter, M.; Rosenblum, K.; Webber, M. J.; Hunt, S. P.; Bliss, T. V. P.; Bramham, C. R. Brain-Derived Neurotrophic Factor Induces Long-Term Potentiation in Intact Adult Hippocampus: Requirement for ERK Activation Coupled to CREB and Upregulation of Arc Synthesis. *J Neurosci* **2002**, *22* (5), 1532–1540. https://doi.org/10.1523/JNEUROSCI.22-05-01532.2002.
(45) Frey, U.; Morris, R. G. Synaptic Tagging and Long-Term Potentiation. *Nature* **1997**, *385* (6616), 533–536. https://doi.org/10.1038/385533a0.

(46) Patton, M. H.; Thomas, K. T.; Bayazitov, I. T.; Newman, K. D.; Kurtz, N. B.; Robinson, C. G.; Ramirez, C. A.; Trevisan, A. J.; Bikoff, J. B.; Peters, S. T.; Pruett-Miller, S. M.; Jiang, Y.; Schild, A. B.; Nityanandam, A.; Zakharenko, S. S. Synaptic Plasticity in Human Thalamocortical Assembloids. *bioRxiv* **2024**, 2024.02.01.578421. https://doi.org/10.1101/2024.02.01.578421.
(47) Zucker, R. S.; Regehr, W. G. Short-Term Synaptic Plasticity. *Annual Review of Physiology* **2002**, *64* (Volume 64, 2002), 355–405. https://doi.org/10.1146/annurev.physiol.64.092501.114547.
(48) Cheng, Q.; Song, S.-H.; Augustine, G. J. Molecular Mechanisms of Short-Term Plasticity: Role of Synapsin Phosphorylation in Augmentation and Potentiation of Spontaneous Glutamate Release. *Front. Synaptic Neurosci.* **2018**, *10*. https://doi.org/10.3389/fnsyn.2018.00033.
(49) France, G.; Volianskis, R.; Ingram, R.; Bannister, N.; Rothärmel, R.; Irvine, M. W.; Fang, G.; Burnell, E. S.; Sapkota, K.; Costa, B. M.; Chopra, D. A.; Dravid, S. M.; Michael-Titus, A. T.; Monaghan, D. T.; Georgiou, J.; Bortolotto, Z. A.; Jane, D. E.; Collingridge, G. L.; Volianskis, A. Differential Regulation of STP, LTP and LTD by Structurally Diverse NMDA Receptor Subunit-Specific Positive Allosteric Modulators. *Neuropharmacology* **2022**, *202*, 108840. https://doi.org/10.1016/j.neuropharm.2021.108840.
(50) Dixon, T. A.; Muotri, A. R. Advancing Preclinical Models of Psychiatric Disorders with Human Brain Organoid Cultures. *Mol Psychiatry* **2023**, *28* (1), 83–95. https://doi.org/10.1038/s41380-022-01708-2.
(51) Havekes, R.; Abel, T. The Tired Hippocampus: The Molecular Impact of Sleep Deprivation on Hippocampal Function. *Curr Opin Neurobiol* **2017**, *44*, 13–19. https://doi.org/10.1016/j.conb.2017.02.005.
(52) Herculano-Houzel, S.; Catania, K.; Manger, P. R.; Kaas, J. H. Mammalian Brains Are Made of These: A Dataset of the Numbers and Densities of Neuronal and Nonneuronal Cells in the Brain of Glires, Primates, Scandentia, Eulipotyphlans, Afrotherians and Artiodactyls, and Their Relationship with Body Mass. *Brain Behavior and Evolution* **2015**, *86* (3–4), 145–163. https://doi.org/10.1159/000437413.
(53) Lavazza, A.; Chinaia, A. A. Human Brain Organoids and Their Ethical Issues. *EMBO reports* **2024**, *25* (1), 13–16. https://doi.org/10.1038/s44319-023-00007-3.
(54) Hartung, T.; Morales Pantoja, I. E.; Smirnova, L. Brain Organoids and Organoid Intelligence from Ethical, Legal, and Social Points of View. *Front. Artif. Intell.* **2024**, *6*. https://doi.org/10.3389/frai.2023.1307613.
(55) Chailangkarn, T.; Trujillo, C. A.; Freitas, B. C.; Hrvoj-Mihic, B.; Herai, R. H.; Yu, D. X.; Brown, T. T.; Marchetto, M. C.; Bardy, C.; McHenry, L.; Stefanacci, L.; Järvinen, A.; Searcy, Y. M.; DeWitt, M.; Wong, W.; Lai, P.; Ard, M. C.; Hanson, K. L.; Romero, S.; Jacobs, B.; Dale, A. M.; Dai, L.; Korenberg, J. R.; Gage, F. H.; Bellugi, U.; Halgren, E.; Semendeferi, K.; Muotri, A. R. A Human Neurodevelopmental Model for Williams Syndrome. *Nature* **2016**, *536* (7616), 338–343. https://doi.org/10.1038/nature19067.
(56) Thomas, C. A.; Tejwani, L.; Trujillo, C. A.; Negraes, P. D.; Herai, R. H.; Mesci, P.; Macia, A.; Crow, Y. J.; Muotri, A. R. Modeling of TREX1-Dependent Autoimmune Disease Using Human Stem Cells Highlights L1 Accumulation as a Source of Neuroinflammation. *Cell Stem Cell* **2017**, *21* (3), 319-331.e8. https://doi.org/10.1016/j.stem.2017.07.009.